A Flexible Selection Scheme for Minimum-Effort Transfer Learning

Amélie Royer
IST Austria
aroyer@ist.ac.at

Christoph Lampert
IST Austria
chl@ist.ac.at

Abstract

Fine-tuning *is a popular way of exploiting knowledge contained in a pre-trained convolutional network for a new visual recognition task. However, the orthogonal setting of transferring knowledge from a pretrained network to a visually different yet semantically close source is rarely considered: This commonly happens with real-life data, which is not necessarily as clean as the training source (noise, geometric transformations, different modalities, etc.).*

To tackle such scenarios, we introduce a new, generalized form of fine-tuning, called ***flex-tuning****, in which any individual* ***unit*** *(*e.g. *layer) of a network can be tuned, and the most promising one is chosen automatically. In order to make the method appealing for practical use, we propose two* ***lightweight and faster selection procedures*** *that prove to be good approximations in practice. We study these selection criteria empirically across a variety of domain shifts and data scarcity scenarios, and show that fine-tuning individual units, despite its simplicity, yields very good results as an adaptation technique. As it turns out, in contrast to common practice, rather than the last fully-connected unit it is best to tune an intermediate or early one in many domain-shift scenarios, which is accurately detected by flex-tuning.*

1. Introduction

Deep convolutional networks have substantially advanced the state of the art in many areas of computer vision. These networks are often interpreted as a feature extraction stage (typically convolutional layers), followed by a small classifier (fully connected layers), and have the ability to learn features from data directly instead of having them hard-coded, as was the case for previous shallow techniques. However, this comes with a cost, as it requires a lot more training data than methods relying on fixed ad-hoc feature extraction. Consequently, it is not surprising that the first successes of deep networks in image classification occurred as large annotated datasets were made available, *e.g.* MNIST [22] for digit recognition (60,000 training samples) or ImageNet [32] for object classification (1.2 million).

When only little available training data is available, however, training a deep feature extraction pipeline from scratch is not possible, as it often leads to severe overfitting. Instead, two main *transfer learning* strategies have emerged, exploiting the fact that deep convolutional networks pre-trained on large datasets are freely available these days [25, 38, 39]: *Either*, one isolates and "freezes" the feature extraction stage of the pre-trained model and then uses the available new data to train only the smaller, less prone to overfitting, classifier stage, *or alternatively*, one fully fine-tunes the model, *i.e.* initializes the network parameters from the pre-trained network, and then trains all layers using the new data, typically only for a few steps, to avoid overfitting. Choosing the best solution depends not only on the *amount of available samples*, though, but also on the *data characteristics*. For example, it has been observed that features learned on large and varied natural images datasets, *e.g.* ImageNet, transfer well to related domains such as aerial or even biomedical images [19]. However, for domains with very different low-level image statistics, *e.g.* sketches, fine-tuning all layers is preferable [3]. Moreover, fine-tuning only a few classification layers is often easier, hence when both options are viable, one might prefer this alternative.

In this work, we argue for a more systematic approach to exploiting pre-trained networks, in situations where the new input domain can *vary greatly in terms of visual appearance*, but its output space shares *similar semantics* with the one the model was pre-trained on. We introduce the idea of *flex-tuning*, a general-purpose transfer learning scheme that leverages the information of an available pre-trained model by fine-tuning a *targeted part of the model*, not necessarily the last layer or all layers, *but any individual layer or block of consecutive layers, selected in a data-dependent way*. In fact, the idea of focusing training resources on specific intermediate layers draws inspiration from an important transfer learning paradigm: It has been consistently observed across various networks and datasets in the literature that early convolutional layers capture elementary local properties of images such as edges or local textures, while middle layers rather represent configurations of several such elements, and the last feature layers extract information about

high-level concepts, such as object parts and their configurations [5, 27, 41]. Thus, in order to adapt, for instance, a network trained on clean natural images to work with noisy ones, we hypothesize it is easier to fine-tune early layers, while for adapting the same network to artistic paintings, focusing on a later layer would be more promising.

Our contribution is three-fold: *First*, we formally define *flex-tuning*, which is a strategy for, given a pre-trained network and a new training dataset, deciding in a data-dependent and automatic way which of the available layers to fine-tune, based on a selection criterion on a held-out validation dataset. *Second*, in order to make flex-tuning more appealing for practical use, we further introduce two variants based on a more efficient selection criterion, called *fast flex-tuning* and *even faster flex-tuning*, that avoid the need to train multiple fine-tuned models for the selection process. *Finally*, we design an extensive experimental setup that covers varied visual domain shifts, data scarcity scenarios and architectures. We show that flex-tuning almost always improves classification accuracy over standard fine-tuning techniques, particularly in settings where fine-tuning all layers is prone to overfitting, such as settings with small sample size and large networks. Furthermore, the (even) faster flex-tuning variants are generally on par with flex-tuning while providing a much lighter selection procedure.

2. Related work

Transferrability of pretrained convolutional networks across visual tasks has been often observed and extensively studied in the computer vision literature [1, 7, 8, 40, 42]. In fact, many state-of-the-art computer vision models are not trained from random initialization, but rely crucially on the re-use of weights from networks pre-trained on large classification tasks, such as ImageNet [32]. Popular examples include the YOLO object detector [31] or fully-convolutional networks for segmentation [24]. In the weakly supervised learning literature, pre-trained features are also used as a compact and semantically meaningful image representation, *e.g*. for image retrieval [2], style transfer [11, 16], colorization [21], or unsupervised part detection [35]. All of these approaches typically aim at transferring knowledge between two tasks that have different output structures but similar input domain appearances and distributions. Closest to our work is [40], which studies the outcome of fine-tuning from different levels of a pre-trained network for the standard transfer learning setting. In comparison, we analyze the effect of tuning a single unit of a pre-trained network, in particular for situations where source and target domains are visually dissimilar but semantically close.

In fact, our interest lies exactly in these orthogonal scenarios, *i.e*. where one has a similar output task, typically multi-class classification, but with –potentially significantly – different *source* and *target* input distributions. This setting resembles, yet differs from, the problem of *domain adaptation* [33, 12, 10], where the goal is to construct a classifier for a, usually unlabelled, target task by exploiting one or more source tasks. In domain adaptation one typically assumes that samples from both source and target domain are available, while in the fine-tuning situation, one only has access to a pre-trained network, not the data distribution it was trained on: This aspect rules out adversarial training [17, 43], paired samples [14], or more generally, exploiting any concrete knowledge from the source distribution to improve predictions on the target domain.

In fact, with the growth of datasets and necessary compute resources, the ability to tune networks without access to the original training data is becoming more and more important: First, when dealing with very large source datasets, training jointly on the source and target domains (as many domain adaptation methods require) is computationally impractical. Second, source training data is sometimes non-public, especially in commercial settings. Third, specific applications require data privacy, preventing public data release, for instance for protecting individuals identities in face recognition models. As such, learning under privacy constraints has become a popular topic in recent years [28].

Recent work has also tackled the problem of domain adaptation by transferring from source to target directly at the pixel level, either via generative models [4] or by identifying simpler causal transformations [29]. Weight tuning methods are nonetheless simpler to use, as they directly act on feature representations, rather than learning a transformation that holds independently of the pre-trained network.

3. Flex-Tuning

Our first contribution in this work is to highlight that *simple and lightweight, but surprisingly effective, model adaptation is possible by fine-tuning the weights of only a single unit in a pretrained network, provided that the right unit is chosen.* Which is the right unit depends crucially, and in a non-trivial way, on the relation between source and target domains as well as on the amount of available data. We propose to identify the best unit automatically in a data-dependent manner using a procedure we call *flex-tuning*.

3.1. Transferring knowledge across domain shifts

First, we formally introduce the transfer learning scenario we are interested in: We are given a pre-trained convolutional network, N, mapping input space X to an output space Y, and whose weights were pre-trained on a training dataset from a *source domain*, that is however not available anymore. Our goal is to learn a network for a *target domain*, for which a new, and potentially small, annotated dataset, $\mathcal{D} \overset{iid}{\sim} \mathcal{P}(X, Y)$, is available. In contrast to the standard *transfer learning* application scenario, we consider practi-

cal settings where the target domain is *semantically* close but *visually* different from the source domain. Here, by semantically close, we mean that the output space of the target task is a subset of the source task. Extending the framework to different output structures, *e.g.* from a classification task to a detection task, would be possible by fine-tuning both the unit selected by flex-tuning and the last fully-connected layer. In this work, we focus on thoroughly analyzing and characterizing the influence of *single units* on transferring knowledge across visually different domains and leave the possibility of combining multiple units for future work.

Nonetheless, the setting we consider encompasses a variety of real-world scenarios, where the source and target domains do not overlap well. For example, we can consider a source network trained on natural images, with the target task of classifying monochrome sketches; or a source network trained on scenes under daylight, that should also operate at night, *etc*. Here we work with images as inputs, and discrete labels as outputs. However, the underlying principles apply equally to other input domains and tasks.

3.2. Flex-tuning

We consider pre-trained multi-layer convolutional architectures, that we decompose into smaller *units*, which we denote by $N = N_L \circ \cdots \circ N_1$. In practice, a unit can simply be a single convolutional or fully-connected layer, or, for more complex architectures, a block of consecutive layers. Intuitively, we think of units N_1 to N_{L-1} as the feature extraction part, while the last layer N_L is the performs the actual classification, however the method applies to arbitrary decompositions. Given such a decomposition, the goal of flex-tuning is to analyze the influence of tuning specific units, not only the last one, for transferring knowledge across domains with different visual appearances. Algorithm 1 describes the steps of flex-tuning in pseudo-code: For each unit of the network, we construct a fine-tuned network $N_{\texttt{ft-}\ell}$ by training the network on the available target data, allowing only the weights of the ℓ-th unit to change, while keeping all the others frozen. We also create a network $N_{\texttt{ft-all}}$, for which all layers are fine-tuned. We train each network with an early stopping criterion, monitoring its performance on the validation set, $\mathcal{D}_{\text{val}}$. This prevents overfitting in a way that is data-dependent and adaptive to each training setting. In fact, different units might have very different numbers of weight parameters, and therefore will often need different numbers of epochs to converge. Finally, we choose the best model out of these $L + 1$ networks by comparing their accuracy on the validation set and output it as the *flex-tuned* model, $N_{\texttt{flex}}$.

3.3. Practicality of the method

Technically, Algorithm 1 performs an exhaustive search over the potential fine-tuned models. Therefore, the existing theoretical results for model selection [34] apply, and we obtain that, in the limit, flex-tuning will indeed choose the best of the possible models. Moreover, the difference between flex-tuning's accuracy estimated from the validation data and the expected accuracy on future data decreases with a rate of $O\left(\sqrt{\frac{\log L}{|\mathcal{D}_{\text{val}}|}}\right)$. In Figure 1, we illustrate flex-tuning's practical use: We apply the proposed method on a small network (5 convolutional and 2 fully connected layers) pre-trained on CIFAR [20] and to be adapted to a subset of the "Quick, Draw!" dataset [6] and a blurred variant of CIFAR, for different sizes of the target training dataset. These preliminary results show that (i) it is often beneficial to fine-tune an intermediate layer rather than the last one and that (ii) well-performing units strongly depend on the dataset and in a non-trivial way, but can be efficiently pinpointed with a simple selection criterion such as flex-tuning.

For deep networks however, flex-tuning can be computationally costly: It requires training as many networks as there are units, plus another one in which all units are fine-tuned. Let us denote the average number of training epochs by E_{one} when fine-tuning a single unit, and by E_{all} when fine-tuning all. Also, let us denote the corresponding average computational cost of one such epoch as c_{one} and c_{all},

Algorithm 1 Flex-Tuning (`flex`)

input target training and validation sets, $\mathcal{D}_{\text{train}}$ and $\mathcal{D}_{\text{val}}$
input pre-trained network with L units, $N = N_L \circ \cdots \circ N_1$

for $\ell = 1, \ldots, L$ **do**
  $N_{\texttt{ft-}\ell} \leftarrow$ fine-tune unit ℓ of N on $\mathcal{D}_{\text{train}}$ until accuracy on $\mathcal{D}_{\text{val}}$ stops improving
  $a_{\texttt{ft-}\ell} \leftarrow$ accuracy of $N_{\texttt{ft-}\ell}$ on $\mathcal{D}_{\text{val}}$
end for
$N_{\texttt{ft-all}} \leftarrow$ fine-tune all units of N on $\mathcal{D}_{\text{train}}$ until accuracy on $\mathcal{D}_{\text{val}}$ stops improving
$a_{\texttt{ft-all}} \leftarrow$ accuracy of $N_{\texttt{ft-all}}$ on $\mathcal{D}_{\text{val}}$
$N_{\texttt{flex}} \leftarrow N_{\texttt{best}}$ for $\texttt{best} \leftarrow \underset{X \in \{1, \ldots, L, \texttt{all}\}}{\arg\max} a_{\texttt{ft-X}}$

output $N_{\texttt{flex}}$

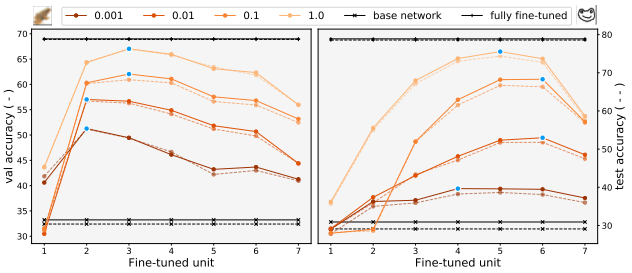

Figure 1. Validation (-) and test (- -) accuracies for fine-tuning a single unit of a pretrained CIFAR network to the Blurry CIFAR (left) and Quick, Draw! (right) datasets. Each line color represents a different subsampling ratio of the target training dataset, while blue markers indicate the unit picked based on validation accuracy.

respectively. Then the total runtime complexity of flex-tuning is $O(LE_{\text{one}}c_{\text{one}} + E_{\text{all}}c_{\text{all}})$. Even when taking into account that typically $E_{\text{all}} > E_{\text{one}}$ and $c_{\text{all}} > c_{\text{one}}$, for reasonably large networks the complexity is often dominated by the computational cost of fine-tuning the network once for each unit. Since ultimately only one of the models is chosen, these computations end up wasted. To address this issue, we introduce two improved selection criteria in the following section to efficiently approximate flex-tuning.

4. Efficient Selection Criteria

4.1. Fast flex-tuning

To overcome the aforementioned computational inefficiency of flex-tuning, we propose a different criterion, *fast flex-tuning*, for selecting the unit to be fine-tuned. It relies on the idea that a given unit's influence can be approximated by *a few feed-forward passes* rather than a full training process. While it does not come with formal guarantees, we found it to work nearly as well as the exhaustive search in practice, while at the same time requiring only 2 networks to be trained instead of $L + 1$. Algorithm 2 describes fast flex-tuning in pseudo-code: The method starts by training one new model, $N_{\texttt{ft-all}}$, by fine-tuning all units of the pre-trained network on the training data available for the target domain. From this, we construct L new networks by *network surgery*. For any $\ell = 1, \ldots, L$, we create a proxy network, $N_{\texttt{prox-}\ell}$, by copying all units from N, except the ℓ-th one, which is copied from the fine-tuned network, $N_{\texttt{ft-all}}$. Clearly, the resulting hybrid networks are not functional models, as the l-th unit and the other units were not trained together. Nevertheless, the construction allows us to derive a measure which of the network units is the most promising candidate for fine-tuning, namely the one that leads to the *biggest improvement in accuracy (if any) when applied to the target domain*. Numerically, we compute the accuracy of each model $N_{\texttt{prox-}\ell}$ on the validation dataset and identify the value for ℓ with highest accuracy. We then create a viable model by fine-tuning the selected unit on the target dataset $\mathcal{D}$. Finally, we output either this model, or the one in which all layers were fine-tuned (which is available as we created it at the beginning of the procedure), depending on which achieved the higher validation accuracy. We report the validation accuracies of the $N_{\texttt{prox-}\ell}$ models for our different experimental settings in the supplemental material.

In comparison to flex-tuning, fast flex-tuning only has to fine-tune two networks instead of $L + 1$. Its runtime complexity is hence $O(E_{\text{one}}c_{\text{one}} + E_{\text{all}}c_{\text{all}})$, thereby providing substantial computational savings for large networks.

4.2. Even faster flex-tuning

In some situations, training from scratch or fine-tuning the complete network is simply computationally too costly:

Algorithm 2 Fast Flex-Tuning (`fast-flex`)

input target training and validation sets, $\mathcal{D}_{\text{train}}$ and $\mathcal{D}_{\text{val}}$
input pre-trained network with L units, $N = N_L \circ \cdots \circ N_1$

$N_{\texttt{ft-all}} \leftarrow$ fine-tune all units of N on $\mathcal{D}_{\text{train}}$ until accuracy on $\mathcal{D}_{\text{val}}$ stops improving
$a_{\texttt{ft-all}} \leftarrow$ accuracy of $N_{\texttt{ft-all}}$ on $\mathcal{D}_{\text{val}}$
for $\ell = 1, \ldots, L$ **do**
  $N_{\texttt{prox-}\ell} \leftarrow N_L \circ \cdots \circ N_{l+1} \circ [N_{\texttt{ft-all}}]_\ell \circ N_{\ell-1} \circ \cdots \circ N_1$
  $a_\ell \leftarrow$ accuracy of $N_{\texttt{prox-}\ell}$ on $\mathcal{D}_{\text{val}}$
end for
$\texttt{best} \leftarrow \arg\max_\ell \; a_\ell,\ \ell \in \{\texttt{1}, \ldots, \texttt{L}\}$
$N_{\texttt{best}} \leftarrow$ fine-tune unit `best` of N on $\mathcal{D}_{\text{train}}$ until accuracy on $\mathcal{D}_{\text{val}}$ stops improving
$a_{\texttt{ft-best}} \leftarrow$ accuracy of $N_{\texttt{best}}$ on $\mathcal{D}_{\text{val}}$
$N_{\texttt{flex}} \leftarrow$ **if** $a_{\texttt{ft-best}} \geq a_{\texttt{ft-all}}$ **then** $N_{\texttt{best}}$ **else** $N_{\texttt{ft-all}}$

output $N_{\texttt{flex}}$

Algorithm 3 Even Faster Flex-Tuning (`faster-flex`)

input target training and validation sets, $\mathcal{D}_{\text{train}}$ and $\mathcal{D}_{\text{val}}$
input pre-trained network with L units, $N = N_L \circ \cdots \circ N_1$

$N_{\texttt{ft-all}} \leftarrow$ fine-tune all units of N on $\mathcal{D}_{\text{train}}$ for a single epoch
for $\ell = 1, \ldots, L$ **do**
  $N_{\texttt{prox-}\ell} \leftarrow N_L \circ \cdots \circ N_{l+1} \circ [N_{\texttt{ft-all}}]_\ell \circ N_{\ell-1} \circ \cdots \circ N_1$
  $a_\ell \leftarrow$ accuracy of $N_{\texttt{prox-}\ell}$ on $\mathcal{D}_{\text{val}}$
end for
$\texttt{best} \leftarrow \arg\max_\ell \; a_\ell,\ \ell \in \{\texttt{1}, \ldots, \texttt{L}\}$
$N_{\texttt{flex}} \leftarrow$ fine-tune unit `best` of N on $\mathcal{D}_{\text{train}}$ until accuracy on $\mathcal{D}_{\text{val}}$ stops improving

output $N_{\texttt{flex}}$

Neither flex-tuning nor fast flex-tuning are applicable, as both require training a network by fine-tuning all units as the first step of their selection process. To overcome this, we propose an even faster variant, as described in Algorithm 3.

Even faster flex-tuning resembles fast flex-tuning in that it selects a unit to be fine-tuned based on the accuracies of different proxy models that are obtained by network surgery, each time preserving $L - 1$ units from the pre-trained source network and replacing the remaining one with its fine-tuned counterpart. The difference lies in that the fine-tuned units are obtained from a network in which all units have been fine-tuned for just a *single epoch*. This results in a total computational runtime of $O(E_{\text{one}}c_{\text{one}} + c_{\text{all}})$. We consider this close to optimal for an adaptive technique, as at least the cost $E_{\text{one}}c_{\text{one}}$ clearly cannot be avoided, if the goal is to produce a network in which at least one unit has been fine-tuned. The drawback of the acceleration is that the *even faster flex-tuning* algorithm does not have access to a reliable estimate of what performance a network with all units fully fine-tuned would have achieved. This is however not relevant here as, by assumption, the computational

method	computational cost
`flex`	$LE_{\text{one}}c_{\text{one}} + E_{\text{all}}c_{\text{all}}$
`fast-flex`	$E_{\text{one}}c_{\text{one}} + E_{\text{all}}c_{\text{all}}$
`faster-flex`	$E_{\text{one}}c_{\text{one}} + c_{\text{all}}$
`ft-fc`	$E_{\text{one}}c_{\text{one}}$
`ft-all`	$E_{\text{all}}c_{\text{all}}$

Table 1. Runtime complexities. L is the number of units in the network, E_{one} and c_{one} are the average number of epochs until early stopping for fine-tuning one unit, and the estimated cost of one such epoch. E_{all} and c_{all} are the analogous quantities when fine-tuning all network units. In general, $E_{\text{all}} > E_{\text{one}}$ and $c_{\text{all}} > c_{\text{one}}$.

budget does not suffice for training such a model anyway.

In summary, even faster flex-tuning is a generalization of fine-tuning the last unit of the network, as is often done in practice, but instead the most promising unit is chosen by a brief selection process. Table 1 summarizes the runtime complexity of all proposed models, as well as the two main baselines we use in our experiments: `ft-fc`, which fine-tunes always the last unit (*i.e*. the fully-connected layer(s)), and `ft-all`, which fine-tunes always all layers.

5. Experiments

In this section, we introduce our experimental setup, covering a large number of domain shifts and data scarcity scenarios. We then describe fine-tuning baselines commonly used in the literature, and compare them to the proposed methods, flex-tuning (`flex`), fast flex-tuning (`fast-flex`) and even faster flex-tuning (`faster-flex`).

5.1. Experimental set-up

We build several domain shift scenarios, ranging from simple parametric transformations to severe visual appearance shifts. In order to explore the impact of data scarcity, we additionally consider several subsampled versions of each target dataset, ranging from a few images per class to hundreds of them. The different settings are thus mainly characterized by: (i) the depth of the base source network, (ii) the size of the target dataset we tune on, and (iii) the type of input domain shift: simple parametric transformations, *e.g*. manipulating color channels, complex (non-trivially invertible) parametric transformations, and general free-range transformations. We summarize our setup in Table 2.

Medium-sized experiments. We first consider a small 4 layers network (which we decompose in 4 one-layer units: 2 convolutional layers followed by 2 fully-connected ones) pretrained on a subset of MNIST training images. We use the remaining samples (except 5000 of them that we keep for validation) to build synthetic domain shifts such as *affine transformations* (randomized or fixed for all images), or *random occlusions*. Second, we build a 7 layers network (7 one-layer units: 5 convolutional and 2 fully connected ones) that we pre-train on half of the CIFAR training set [20]. As target domains, we consider several synthetic transformations of the remaining samples, as well as a subset of the QuickDraw dataset [6]: We restrict ourselves to the object classes they have in common, *i.e*. all CIFAR classes except for "deer". We also consider the converse setting, *i.e*. pre-training on QuickDraw and using as target domains CIFAR and synthetically generated blurry and noisy QuickDraw samples. Since both aforementioned architectures have two fully connected layers, we consider two baselines, `ft-fc` (1) and `ft-fc` (2), corresponding to fine-tuning only the last, or the last two fully-connected layers respectively.

Large-scale setting. Finally, we consider two large-scale settings using the Inception2 architecture [13, 39, 37]. We decompose the model so as to not separate layers belonging to the same Inception module, which results in 13 units, the last one being the single fully-connected classification layer of the architecture. We first experiment on synthetic transformations of natural images. For this setting, we use a network pretrained on ILSVRC2012-train. We then split ILSVRC2012-val in three parts. 25k images are used to create target datasets, 5k are kept for validation and the remaining 20k are used for testing. Second, we consider the more challenging setting of stylistic transformations using the PACS dataset [23], initially introduced for the task of domain generalization: We use art paintings, cartoons and sketches, as target domains, which we further split into train/val/test sets. In this setting, the target task is a subset of the source ILSVRC classification task (ignoring the "person" class in PACS as it does not have an equivalent).

Baselines. We first consider the two most common transfer learning schemes as baselines. Starting with a network initialized with the same weights and architectures as the source pre-trained network, N: (i) `ft-all` consists in fine-tuning *all* layers $N_1, \dots N_L$ on the training set $\mathcal{D}$ from the target domain, and (ii) `ft-fc`, which corresponds to fine-tuning only the last *fully-connected* units of the network, while keeping earlier units frozen. We also consider using scaling and shifting operations as in [36] and refer to this baseline as `ft-ss`: It consists in fine-tuning the last classification layer as well as lightweight kernel-scaling and bias-shifting parameters at every layer. Thus `ft-ss` acts on all levels of the architecture, but requires few additional learning parameters, hoping to prevent overfitting problems.

Training. We measure performance as `top-1` classification accuracy, and `top-5` for ILSVRC-based domains. We use the same hyperparameters as were used during training of the base source network. As is common, for finetuning, we use a lower base learning rate: 10^{-3} for the small convolutional networks, and 10^{-4} for the Inception2 networks. We train all models using the Adam [18] optimizer. As mentioned previously, we also employ an early stopping criterion based on validation accuracy, regularly computed

Source	Target domains
 **MNIST** (subset) [22] 25k images 10 classes 4-layers top-1: 0.989	 **Blurry** top-1: 0.748  **Occluded** top-1: 0.581  **MNIST-M** [9] top-1: 0.439  **Transform (random)** top-1: 0.322  **SVHN** [26] top-1: 0.211  **Transform (fixed)** top-1: 0.160 **ratios** ∼ 3, 30, 300 and 3k images per class
 **CIFAR** (subset) [20] 18k images 9 classes 7-layers top-1: 0.738	 **Noisy** top-1: 0.540  **Blurry** top-1: 0.324  **QuickDraw** [6] top-1: 0.291 **ratios** ∼ 2, 20, 200 and 2k images per class
 **ILSVRC** [32] **('12 train split)** 1M images 1000 classes Inception2 top-5: 0.918	 **YUV** top-5: 0.841  **Fixed rotation** top-5: 0.743  **Fixed scaling (symmetric pad)** top-5: 0.519  **Fixed scaling (stretch pad)** top-5: 0.440  **HSV** top-5: 0.384 **ratios** ∼ 2, 12 and 25 images per class
	 **Art** top-1: 0.532  **Cartoon** top-1: 0.346  **Sketch** top-1: 0.142 **ratios** ∼ 2, 20 and 200 images per class

Table 2. Source domains and architectures (*left*) we consider, with the corresponding target domains (*right*) and the training dataset **subsampling ratios** we consider, as the average number of images per class: the last entry corresponds to the full dataset size.

during training (every 5-10 epochs). This also dampens the negative effect of overfitting in scenarios that are overly prone to it (*e.g.* `ft-all` with small sample size and a large network). Finally, in the very scarce data setting ($\sim$ 1 image per class) we report metrics averaged over 20 runs, to avoid a potential bias towards the sampled training images.

5.2. Main results

In Table 3 we compare the proposed method and baselines on the MNIST, CIFAR and ILSVRC-based settings, for one subsampling ratio of the target training set. Results for other ratios show similar trends and are available in the supplemental material. For the more challenging PACS scenario, which exhibits both a strong visual shift and slight semantic labels shift from the source task, we report complete results across all subsampling ratios.

We observe that `flex` outperforms fine-tuning baselines in almost all settings. It very rarely loses to the `ft-fc` baseline, but is sometimes tied with `ft-all`, which is a subcase of `flex` and `fast-flex` through the selection criterion. More precisely, over all subsampling ratios and domain shifts we have in total 72 transfer scenarios. Out of these, the two overall best methods are `flex` and `fast-flex`, achieving best accuracy 60 and 41 times respectively. Compared to this, `ft-all` only reaches the best accuracy 26 times, mostly for large sample size and medium-sized networks. It consistently loses due to overfitting in other scenarios. More interestingly, in terms of absolute values, we observe that when `flex` strictly wins, *i.e.* when it reaches the best accuracy and not in a tie with `ft-all`, it typically does so by a higher margin than in the reverse scenario, *i.e.* when one of the baselines strictly wins. We detail our main observations in the rest of the section.

Comparison to baselines. In the medium network or large sample size settings, flex-tuning expectedly generally chooses to fine-tune all layers, *i.e.* `flex` recovers `ft-all`. However, as the dataset size to network depth ratio decreases, fine-tuning all layers becomes more prone overfitting. In that case, `flex` prefers to fine-tune a specific unit, which generally performs better than the `ft-fc` baseline. More generally, the behavior of `ft-fc` strongly correlates with the difficulty of the input domain shift: it performs best in settings where the source domain early layers generalize well to the target domain, *e.g.* in the noisy CIFAR setting where the small additive random noise does not impact activations significantly. When the domain shift is more pronounced however, `ft-fc` is often outperformed by `flex`, `fast-flex` and `faster-flex` which pick a more adequate unit to tune. This shows there is a benefit to having the method pick the best unit to fine-tune, rather than restricting transfer learning to the last fully-connected layers. These conclusions also hold for `ft-ss`, although it provides a much stronger baseline than `ft-fc` and is sometimes on-par or outperforms the faster flextuning variants. However, its performance seems to depend on the type of domain shift: For instance, `ft-ss` performs moderately well on the colorized-ILSVRC setting. We attribute it to the fact that this setting involves a recombination of the channels which is not well captured by affine transformations of the parameters. Finally, `flex` and its variants are easier to implement in practice as they do not introduce additional parameters nor require to know how layers actually operate.

Selecting the best unit. We observe that the most promising unit selected by flex-tuning is often an intermediate one and does not follow an obvious pattern, showing that different domain shifts affect layer representations at different depths of the architecture: This is illustrated in Figure 2. On the same figure, we see that fast flex-tuning and even faster flex-tuning are good approximations of flex-tuning as

ILSVRC	flex			ft-		
	flex	fast	faster	fc	ss	all
ratio: 2 images per class						
Art (0.53)	**0.669**	**0.703**	**0.655**	0.626	0.630	0.628
Cartoon (0.32)	0.639	**0.683**	0.593	0.618	0.647	0.507
Sketch (0.14)	**0.625**	**0.606**	0.414	0.554	0.581	0.337
ratio: 20 images per class						
Art (0.53)	**0.870**	**0.851**	**0.861**	0.729	0.849	0.724
Cartoon (0.32)	**0.912**	**0.893**	0.841	0.820	0.887	0.709
Sketch (0.14)	**0.852**	0.638	0.638	0.766	0.801	0.542
ratio: 200 images per class						
Art (0.53)	**0.906**	**0.906**	0.823	0.791	0.887	0.746
Cartoon (0.32)	**0.958**	0.956	0.952	0.868	0.956	0.925
Sketch (0.14)	**0.924**	**0.924**	0.890	0.767	0.916	0.875

MNIST	flex			ft-			
	flex	fast	faster	fc (1)	fc (2)	ss	all
Blurry (0.75)	0.926	0.926	0.926	0.921	**0.928**	**0.928**	0.921
Occluded (0.58)	**0.806**	**0.806**	0.801	0.785	0.801	0.792	**0.806**
MNIST-M (0.44)	**0.683**	**0.683**	0.671	0.615	0.670	0.675	**0.683**
SVHN (0.21)	**0.669**	**0.669**	0.572	0.451	0.595	0.657	**0.669**
Transf. (rnd) (0.32)	**0.644**	**0.644**	**0.644**	0.573	0.638	0.624	0.625
Transf. (fix) (0.16)	**0.908**	0.887	0.879	0.839	0.875	0.866	0.887

CIFAR	flex			ft-			
	flex	fast	faster	fc (1)	fc (2)	ss	all
Blurry (0.32)	**0.577**	**0.577**	0.512	0.444	0.501	0.569	**0.577**
Noisy (0.54)	**0.624**	**0.624**	**0.624**	0.583	0.597	0.618	0.621
QuickDraw (0.29)	0.518	0.517	0.517	0.475	**0.525**	0.495	0.501

QuickDraw	flex			ft-			
	flex	fast	faster	fc (1)	fc (2)	ss	all
Blurry (0.19)	0.642	0.631	0.560	0.426	0.468	**0.707**	0.631
Noisy (0.63)	0.801	0.801	0.795	0.788	0.792	**0.805**	0.801
CIFAR (0.20)	**0.424**	**0.424**	0.401	0.333	0.347	0.388	**0.424**

ILSVRC	flex			ft-		
	flex	fast	faster	fc	ss	all
YUV (0.84)	**0.893**	**0.893**	**0.893**	0.835	0.699	0.808
HSV (0.38)	**0.856**	**0.856**	**0.856**	0.533	0.646	0.687
Scaling (stretch) (0.44)	**0.724**	**0.696**	**0.696**	0.502	0.584	0.653
Scaling (sym.) (0.52)	**0.770**	**0.757**	**0.757**	0.663	0.650	0.716
Rotation (0.74)	**0.826**	**0.832**	**0.812**	0.667	0.652	0.771

Table 3. Break-down of results comparing our proposed `flex`, `fast-flex` and `faster-flex`, to fine-tuning baselines, `ft-all` and `ft-fc`. In each table, the first column lists each *source*→ *target* domain shifts, with the base accuracy reached by the pretrained source network on the target test set. Bold entries indicate the score is better than that of *all* baselines (`ft-`). For space reason, we only report results for a specific subsampling ratio for settings other than PACS (roughly 30 images per class for MNIST, 20 for CIFAR, 12 for ILSVRC). Full results are in the supplemental material.

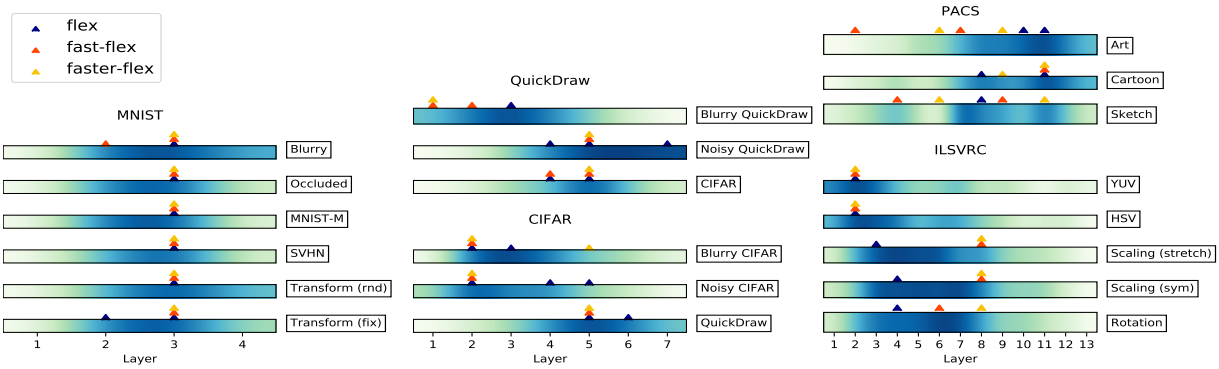

Figure 2. Individual units selected by `flex`, `fast-flex` and `faster-flex`, based on *validation* set accuracy. Triangles denote actual picks for `flex`, `fast-flex` (if ignoring the option to fine-tune all units) and `faster-flex`. The background values is obtained by summing the selection ranks of each unit across ratios, based on their *test performance*: in other words, the darker the color, the best performance fine-tuning this unit yields on the test set. We observe that flex-tuning's selection criterion generally chooses the best performing unit. The two variants' choices are more scattered, but overall positively correlate with flex-tuning's decisions.

they often pick similar units. Similarly in Table 3 we observe that they both often outperform fine-tuning baselines, although still being somewhat subpar to `flex`. This shows that only a few gradient updates, as is done in even faster flex-tuning, are enough to pin-point relevant units.

Effect of the domain shift on `flex`. From Figure 2, we distinguish three input domain shifts categories: For local *pixel-level transformations*, such as noisy CIFAR, or YUV/HSV ILSVRC, flex-tuning tends to choose early units. This coincides with the fact that (i) early layers are most affected by local pixel-level changes, and (ii) such transformations are easy to correct in early layers: *e.g.* YUV is a linear transformation of RGB. For *geometric affine transformations*, flex-tuning picks more central units of the architecture. In fact, such transformations do not change the global appearance of images and, moreover, most modern deep learning architecture are trained for invariance to small geometric manipulations (*e.g.* flip, rotations) via synthetic data augmentation, hence earlier layers are more easily transferable across these domain shifts. The free-transform scenarios are harder to generalize: First, we observe that natural images features transfer particularly well across various domains. As such, flex-tuning often picks later layer in the architecture for general transforms scenarios with natural images as their source domain, *e.g. photo*→ {*art, cartoon, sketch*}. However, this does not seem to be

	YUV	HSV	Art	Cartoon	Sketch
ft-fc	0.80	0.47	0.66	0.53	0.39
ft-all	0.75	0.52	0.80	0.83	0.85
flex	0.85	0.85	0.88	0.86	0.86

Table 4. mAP@10 retrieval results for the fine– and flex-tuned network embeddings, queried against the source domain embeddings

the case in the reverse scenario, *e.g. QuickDraw→ CIFAR* and *MNIST→ SVHN*, which indicates that features learned from the simple structure and particular distribution of binary sketches do not generalize as well to natural images. Second, in some complex settings such as PACS, it can be the case that *two non-consecutive units* are good fine-tuning candidates. This suggests that units sometimes interact in complex patterns and that considering combination of units rather than single ones is an interesting future direction.

5.3. Retrieval Experiments

A benefit of fine-tuning the last layer only is that it preserves a common feature representation across domains. However this property breaks in our setting: Images visually different from the training set fall out of the usual operation zone of the feature extractor. One can still learn a good classifier from these features [30], but the representations themselves are meaningless with respect to the initial source domain. On the other hand, tuning an intermediate unit instead could help to "mend" the representation. To evaluate this, we use a retrieval experiment: We extract features for the initial source validation domain through the source network, and for the target domain through the flex-tuned or finetuned network. For each target sample, we retrieve its top-k nearest neighbors in the source domain and consider them correctly retrieved if they share the same semantic class, and evaluate the average precision (AP@k). For space reasons, we only report AP@10, on the most challenging scenarios, in Table 4. Full results are reported in the supplemental material. The results follow our previous observations: For small networks (MNIST, CIFAR) the result of fine-tuning all layers is often better aligned with the initial representations. However for the larger architectures, tuning an intermediate unit better recover the initial source embedding space as shown in Table 4.

5.4. Towards pixel-level adaptation

An alternative to tuning a pre-trained network is to instead learn to map target samples back to the source domain while keeping the network's weights untouched; This has the advantage of only depending on the domain shift and not on the architecture. Such *image-to-image mapping* modules have been studied for domain adapation, but typically require data from both source and target domains [4, 43].

Building on this idea, we introduce an *image-to-image transformation unit* as a pre-processing module before the feature extraction phase of the pre-trained source network.

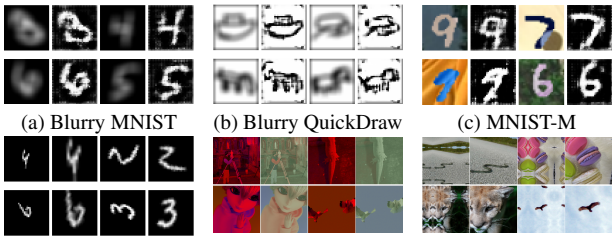

(a) Blurry MNIST (b) Blurry QuickDraw (c) MNIST-M

(d) Transformed (rnd) (e) YUV (1 layer) (f) Scaling (symmetric)

Figure 3. Example images generated by the pre-processing module. For each pair, the left image is the input from the target domain and the right one is the pre-processed output.

The resulting architecture is considered as a new model selection option for flex-tuning, where only the image-to-image unit's weights are trained and the rest of the network is frozen. We implement this image-to-image unit as a small Pix2Pix network [14] except in a few secnarios where we leverage our prior knowledge of the domain shift: For example, color channel transformations occur pixel-wise, thus we build the preprocessing module for YUV and HSV ILSVRC with 1x1 convolutions. Similarly, for geometric transforms, we use a Spatial Transformer Network [15]. Figure 3 shows exemplary outputs of the learned image-to-image units. Quantitative results are in the supplemental material. The specialized pre-processing modules performs very well for simple parametric transformations, and results are also encouraging on simple domain shifts such as *blur*, *noise* and added *random background*. We believe this to be a consequence of the skip connections in the Pix2Pix architecture, which enforce local pixel constraints between the input and output. In all these succesful cases, flex-tuning's selection criterion also selects the image-to-image unit as the most promising unit to tune. For complex transformations, *e.g. photo→ sketch*, the pre-processing module performs poorly. Nevertheless, flex-tuning is able to notice this and falls back to one of the other units to adapt.

6. Conclusions

We introduce a new transfer learning method for neural networks, *flex-tuning*, that adapts a pre-trained network to a new domain by tuning just a single network unit (*e.g.* a layer or block layers). Our experiments on a variety of scenarios show that this is a surprisingly strong adaptation technique, as long as the right unit is chosen. Specifically, we study the case where output classes stay consistent but the input data characteristics change, potentially dramatically, *e.g.* from images to sketch drawings. We find that, contrary to common practice, it is then rarely the last fully-connected unit, but rather an intermediate or early unit, that leads to the best adaptation results, and *flex-tuning* reliably identifies it. We also introduce two accelerated variants that perform almost equally good but are significantly more computationally efficient in selecting the unit to be fine-tuned.

References

[1] H. Azizpour, A. S. Razavian, J. Sullivan, A. Maki, and S. Carlsson. Factors of transferability for a generic ConvNet representation. *IEEE Transactions on Pattern Analysis and Machine Intelligence (T-PAMI)*, 2016. 2

[2] A. Babenko and V. S. Lempitsky. Aggregating local deep features for image retrieval. In *International Conference on Computer Vision (ICCV)*, 2015. 2

[3] P. Ballester and R. M. Araujo. On the performance of GoogLeNet and AlexNet applied to sketches. In *Conference on Artificial Intelligence (AAAI)*, 2016. 1

[4] K. Bousmalis, N. Silberman, D. Dohan, D. Erhan, and D. Krishnan. Unsupervised pixel-level domain adaptation with generative adversarial networks. In *Conference on Computer Vision and Pattern Recognition (CVPR)*, 2017. 2, 8

[5] S. A. Cadena, M. A. Weis, L. A. Gatys, M. Bethge, and A. S. Ecker. Diverse feature visualizations reveal invariances in early layers of deep neural networks. In *European Conference on Computer Vision (ECCV)*, 2018. 2

[6] S. Cheema, S. Gulwani, and J. LaViola. QuickDraw: Improving drawing experience for geometric diagrams. In *Conference on Human Factors in Computing Systems (SIGCHI)*, 2012. 3, 5, 6

[7] B. Chu, V. Madhavan, O. Beijbom, J. Hoffman, and T. Darrell. Best practices for fine-tuning visual classifiers to new domains. In *ECCV Workshop TASK-CV: Transferring and Adapting Source Knowledge in Computer Vision*, 2016. 2

[8] J. Donahue, Y. Jia, O. Vinyals, J. Hoffman, N. Zhang, E. Tzeng, and T. Darrell. DeCAF: A deep convolutional activation feature for generic visual recognition. In *International Conference on Machine Learing (ICML)*, 2014. 2

[9] Y. Ganin and V. Lempitsky. Unsupervised domain adaptation by backpropagation. In *International Conference on Machine Learing (ICML)*, 2015. 6

[10] Y. Ganin, E. Ustinova, H. Ajakan, P. Germain, H. Larochelle, F. Laviolette, M. Marchand, and V. Lempitsky. Domain-adversarial training of neural networks. *Journal of Machine Learning Research (JMLR)*, 2016. 2

[11] L. A. Gatys, A. S. Ecker, and M. Bethge. Image style transfer using convolutional neural networks. In *Conference on Computer Vision and Pattern Recognition (CVPR)*, 2016. 2

[12] R. Gopalan, R. Li, and R. Chellappa. Domain adaptation for object recognition: An unsupervised approach. In *International Conference on Computer Vision (ICCV)*, 2011. 2

[13] S. Ioffe and C. Szegedy. Batch normalization: Accelerating deep network training by reducing internal covariate shift. In *Journal of Machine Learning Research (JMLR)*, 2015. 5

[14] P. Isola, J.-Y. Zhu, T. Zhou, and A. A. Efros. Image-to-image translation with conditional adversarial networks. In *Conference on Computer Vision and Pattern Recognition (CVPR)*, 2017. 2, 8

[15] M. Jaderberg, K. Simonyan, A. Zisserman, and K. Kavukcuoglu. Spatial transformer networks. In *Conference on Neural Information Processing Systems (NIPS)*, 2015. 8

[16] J. Johnson, A. Alahi, and L. Fei-Fei. Perceptual losses for real-time style transfer and super-resolution. In *European Conference on Computer Vision (ECCV)*, 2016. 2

[17] T. Kim, M. Cha, H. Kim, J. K. Lee, and J. Kim. Learning to discover cross-domain relations with generative adversarial networks. In *International Conference on Machine Learing (ICML)*, 2017. 2

[18] D. P. Kingma and J. L. Ba. Adam: a method for stochastic optimization. In *International Conference on Learning Representations (ICLR)*, 2015. 5

[19] S. Kornblith, J. Shlens, and Q. V. Le. Do better ImageNet models transfer better? In *Conference on Computer Vision and Pattern Recognition (CVPR)*, 2019. 1

[20] A. Krizhevsky. Learning multiple layers of features from tiny images. Technical report, University of Toronto, 2009. 3, 5, 6

[21] G. Larsson, M. Maire, and G. Shakhnarovich. Learning representations for automatic colorization. In *European Conference on Computer Vision (ECCV)*, 2016. 2

[22] Y. LeCun and C. Cortes. MNIST handwritten digit database. http://yann.lecun.com/exdb/mnist/. 1, 6

[23] D. Li, Y. Yang, Y.-Z. Song, and T. M. Hospedales. Deeper, broader and artier domain generalization. In *International Conference on Computer Vision (ICCV)*, 2017. 5

[24] J. Long, E. Shelhamer, and T. Darrell. Fully convolutional networks for semantic segmentation. In *Conference on Computer Vision and Pattern Recognition (CVPR)*, 2015. 2

[25] Deep Learning Model Zoo. https://modelzoo.co/. 1

[26] Y. Netzer, T. Wang, A. Coates, A. Bissacco, B. Wu, and A. Y. Ng. Reading digits in natural images with unsupervised feature learning. In *NIPS Workshop on Deep Learning and Unsupervised Feature Learning*, 2011. 6

[27] C. Olah, A. Mordvintsev, and L. Schubert. Feature visualization. *Distill*, 2017. https://distill.pub/2017/feature-visualization. 2

[28] N. Papernot, M. Abadi, Ú. Erlingsson, I. J. Goodfellow, and K. Talwar. Semi-supervised knowledge transfer for deep learning from private training data. In *International Conference on Learning Representations (ICLR)*, 2017. 2

[29] G. Parascandolo, N. Kilbertus, M. Rojas-Carulla, and B. Schölkopf. Learning independent causal mechanisms. In *International Conference on Machine Learing (ICML)*, 2018. 2

[30] A. Rahimi and B. Recht. Weighted sums of random kitchen sinks: Replacing minimization with randomization in learning. In *Conference on Neural Information Processing Systems (NIPS)*, 2008. 8

[31] J. Redmon, S. K. Divvala, R. B. Girshick, and A. Farhadi. You only look once: Unified, real-time object detection. In *Conference on Computer Vision and Pattern Recognition (CVPR)*, 2016. 2

[32] O. Russakovsky, J. Deng, H. Su, J. Krause, S. Satheesh, S. Ma, Z. Huang, A. Karpathy, A. Khosla, M. Bernstein, A. C. Berg, and L. Fei-Fei. ImageNet Large Scale Visual Recognition Challenge. *International Journal of Computer Vision (IJCV)*, 2015. 1, 2, 6

[33] K. Saenko, B. Kulis, M. Fritz, and T. Darrell. Adapting visual category models to new domains. In *European Conference on Computer Vision (ECCV)*, 2010. 2

[34] S. Shalev-Shwartz and S. Ben-David. *Understanding machine learning: From theory to algorithms*. Cambridge University Press, 2014. 3

[35] M. Simon and E. Rodner. Neural activation constellations: Unsupervised part model discovery with convolutional networks. In *International Conference on Computer Vision (ICCV)*, 2015. 2

[36] Q. Sun, Y. Liu, T.-S. Chua, and B. Schiele. Meta-transfer learning for few-shot learning. In *Conference on Computer Vision and Pattern Recognition (CVPR)*, 2019. 5

[37] C. Szegedy, W. Liu, Y. Jia, P. Sermanet, S. Reed, D. Anguelov, D. Erhan, V. Vanhoucke, and A. Rabinovich. Going deeper with convolutions. In *Conference on Computer Vision and Pattern Recognition (CVPR)*, 2015. 5

[38] TensorFlow Hub. https://www.tensorflow.org/hub/. 1

[39] TensorNets. https://github.com/taehoonlee/tensornets. 1, 5

[40] J. Yosinski, J. Clune, Y. Bengio, and H. Lipson. How transferable are features in deep neural networks? In *Conference on Neural Information Processing Systems (NIPS)*, 2014. 2

[41] M. D. Zeiler and R. Fergus. Visualizing and understanding convolutional networks. In *European Conference on Computer Vision (ECCV)*, 2014. 2

[42] R. Zhang, P. Isola, A. A. Efros, E. Shechtman, and O. Wang. The unreasonable effectiveness of deep features as a perceptual metric. In *Conference on Computer Vision and Pattern Recognition (CVPR)*, 2018. 2

[43] J.-Y. Zhu, T. Park, P. Isola, and A. A. Efros. Unpaired image-to-image translation using cycle-consistent adversarial networks. In *International Conference on Computer Vision (ICCV)*, 2017. 2, 8

Supplemental Material for paper ID 628
A Flexible Selection Scheme for Minimum-Effort Transfer Learning

This supplemental material contains complementary experiments for the paper "Flex-Tuning: A Flexible and Automatic Selection Scheme for Transfer Learning". The first section contains the detailed validation accuracies for each of the N_{prox} models which are built during the model selection phase of the fast and faster flextuning variants. In the following sections, we report detailed results for each of our experimental settings; This includes the dataset construction, experimental settings, and quantitative and qualitative results, as well as for the retrieval experiments. We first detail our experiments on a small illustrative 4-layers network on MNIST [9] in Section 2. In Section 3, we report on experiments for a middle size 7-layers network, using the CIFAR-10 [8] and Quick, Draw! [1] datasets. Finally, we describe large-scale experiments with the Inception2 architecture on the ILSVRC [13] and PACS [10] datasets in Section 4 and Section 5, respectively.

In Section 6, we report complete results of our information retrieval experiments. Finally, the last section contains results for the transfer learning baseline described in [2]. In our experiments, it did not perform much better than the standard finetuning baseline therefore we did not include it in the main manuscript.

1. Model selection in fast and faster flextuning

As described in the main manuscript, the proposed *fast flextuning* variant selects the best unit to tune by the following "network surgery": The method starts by training one new model, $N_{\texttt{ft-all}}$, by fine-tuning all units of the pre-trained network on the training data available for the target domain (In the *faster* variant, this model is only trained for one epoch). From this, we construct L new networks: for any $l = 1, \ldots, L$, we create a proxy network, $N_{\texttt{prox-}l}$, by copying all units from N, except the l-th one, which is copied from the fine-tuned network, $N_{\texttt{ft-all}}$.

The construction allows us to derive a measure which of the network units is the most promising candidate for fine-tuning, namely the one that leads to the *biggest improvement in accuracy (if any) when applied to the target domain*. Numerically, we compute the accuracy of each model $N_{\texttt{prox-}l}$ on the validation dataset and identify the value for l with highest accuracy. We report validation accuracies of these models in Figure 1 to Figure 4.

Each of this plot represents the validation accuracy versus layer l obtained by model $N_{\texttt{prox-}l}$. Each line corresponds to a different source→domain shift setting. The unit selected by the method is highlighter in white. Finally, the point at $l = 0$ corresonds to applying the source pre-trained network directly to the target samples.

In general, we note that the selected unit is rather consistent across data subsamling ratios (left to right plot). However, the different domain shifts (different lines) vary quite a lot. For some settings, for instance YUV or HSV ILSVRC, the influence of network surgery is clear and significantly highlight a particular unit. While for more complex scenarios such as *photo→art*, several units have strong influence. This phenomenon is even more present in the faster flextuning plots.

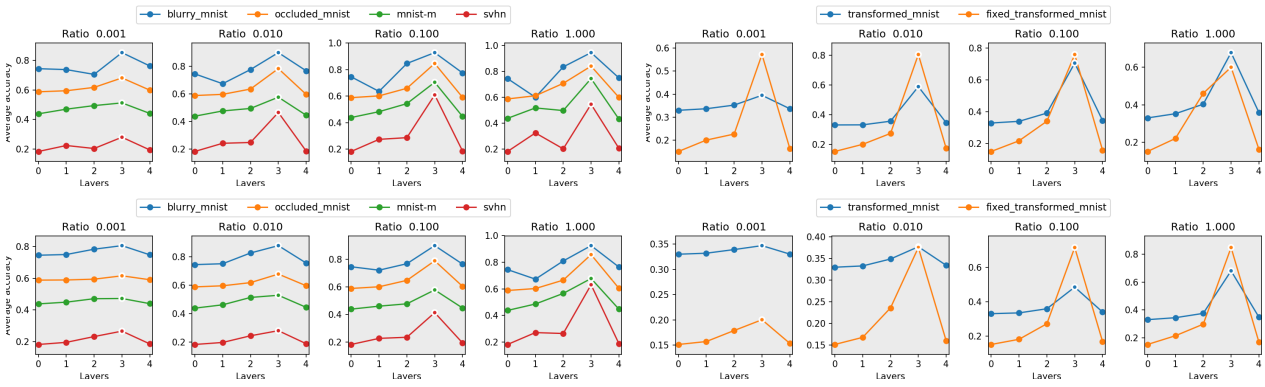

Figure 1: $N_{\texttt{prox-}l}$ validation accuracies for the fast (top) and faster (bottom) flextuning model selection criterion for MNIST

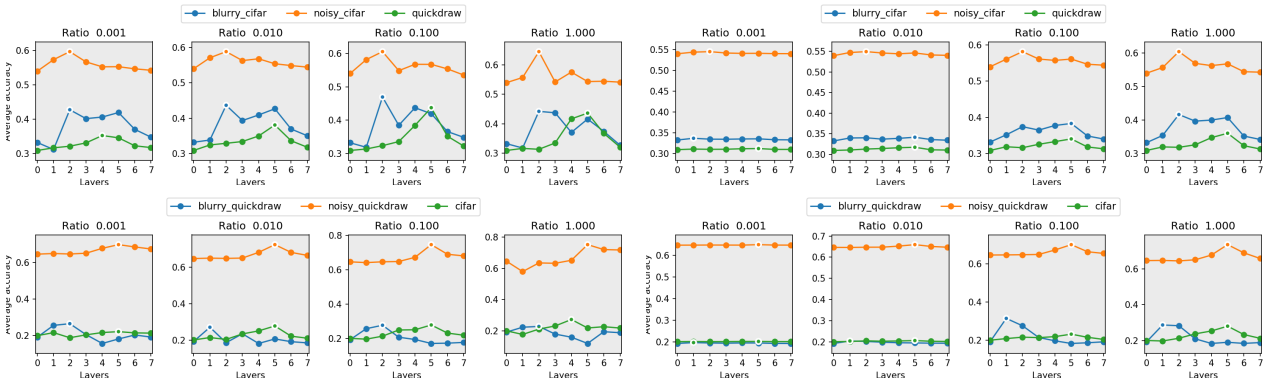

Figure 2: $N_{\text{prox-}l}$ validation accuracies for the fast (left) and faster (right) flextuning model selection criterion for CIFAR and Quickdraw

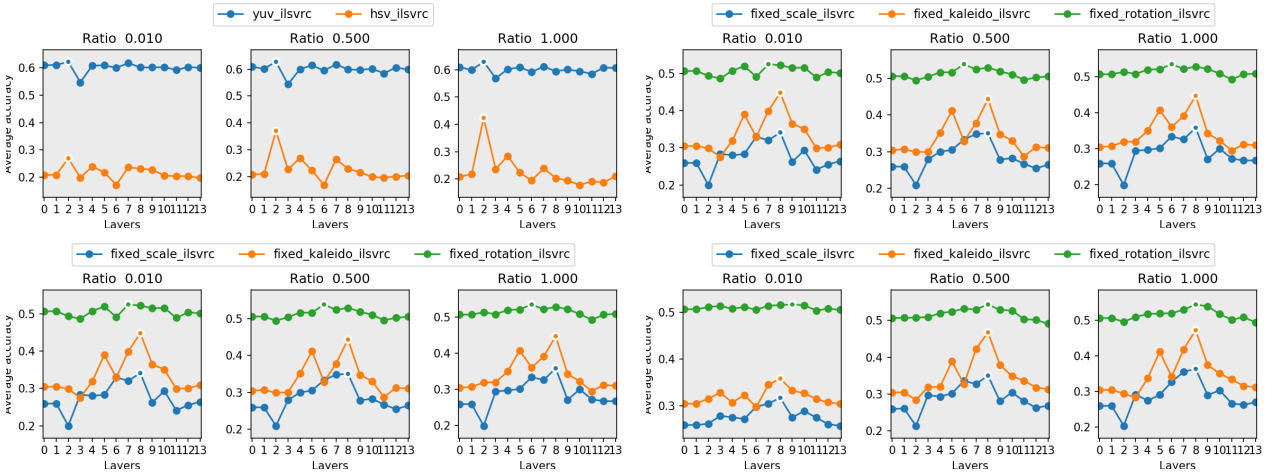

Figure 3: $N_{\text{prox-}l}$ validation accuracies for the fast (top) and faster (bottom) flextuning model selection criterion for ILSVRC

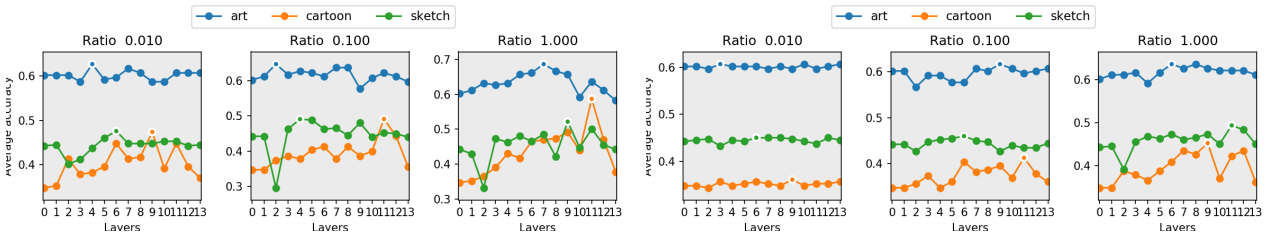

Figure 4: $N_{\text{prox-}l}$ validation accuracies for the fast (lefgt) and faster (faster) flextuning model selection criterion for PACS

2. MNIST experiments

Datasets and base architecture. We build a network composed of 2 convolutional layers followed by 2 fully connected layers, with ReLU activations. We pretrain this network on a random subset of 25000 images from the original MNIST training set, achieving **0.989** top-1 accuracy on the test set. We split the remaining images in a training set of 30000 images, $\mathcal{D}_{\text{train}}$, and a validation set of 5000 images, $\mathcal{D}_{\text{val}}$, which we use to generate synthetic transforms of MNIST as target domains, avoiding any overlap with the dataset used for pretraining. We denote by $\mathcal{D}_{\text{test}}$ the original MNIST test set of 10000 images.

We first build **Blurry MNIST** by applying a Gaussian blur with a kernel of length 8 and standard deviation $\sigma = 1$ on all images in $\mathcal{D} = (\mathcal{D}_{\text{train}}, \mathcal{D}_{\text{val}}, \mathcal{D}_{\text{test}})$. We also construct **Occluded MNIST** by randomly occluding a patch of size 14x14 pixels on each image in $\mathcal{D}$. The random patches coordinates are generated only once hence the dataset stays the same across runs. We also generate two **geometric transforms** of MNIST by creating affine transformations, either one fixed transformation for all images or a different random transformation for each image, and applying them to $\mathcal{D}_{\text{train}}$, $\mathcal{D}_{\text{val}}$ and $\mathcal{D}_{\text{test}}$. These affine transforms are generated as a rescaling operation ($s \in [0.4, 1.0]$) followed by a translation, randomly sampled from any value that keeps the sampled patch in the original 28x28 pixels canvas, and finally a rotation, with angle $\theta \in [-1.5, 1.5]$ radians. As for more complex transformations, we follow the same construct as for the **MNIST-M** dataset [5] by inlaying random background patches from the BSD [11] dataset on $\mathcal{D}_{\text{train}}$, $\mathcal{D}_{\text{val}}$ and $\mathcal{D}_{\text{test}}$. We also experiment on **SVHN** [12] as a target domain, which we split into 63k training images, 10k validation images, and keep the original test set of 26k images. In this setting, we also resize images to size 28x28 pixels to match the other datasets. In order to evaluate the impact of data scarcity, we create subsampled versions of each target training dataset by randomly sampling images with ratios 0.001, 0.01 and 0.1.

Source domain
MNIST (subset)
25k images, 10 classes
4-layers network
top-1: 0.989

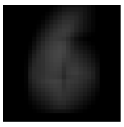

Blurry
top-1: 0.748
$\cos_{\text{src}}$: 0.101
$\cos_{\text{pc}}$: 0.116
ipc: 3-30-300-3k

Occluded
top-1: 0.581
$\cos_{\text{src}}$: 0.051
$\cos_{\text{pc}}$: 0.067
ipc: 3-30-300-3k

MNIST-M [4]
top-1: 0.439
$\cos_{\text{src}}$: 0.128
$\cos_{\text{pc}}$: 0.210
ipc: 3-30-300-3k

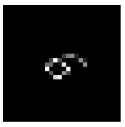

Random transform
top-1: 0.322
$\cos_{\text{src}}$: 0.283
$\cos_{\text{pc}}$: 0.375
ipc: 3-30-300-3k

SVHN [12]
top-1: 0.211
$\cos_{\text{src}}$: 0.248
$\cos_{\text{pc}}$: 0.435
ipc: 6-60-600-6k

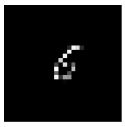

Fixed transform
top-1: 0.160
$\cos_{\text{src}}$: 0.443
$\cos_{\text{pc}}$: 0.531
ipc: 3-30-300-3k

Table 1: Experimental setup for the MNIST source domain (left). For each target domain (right), we report the average number of training images per class (ipc) for each data subsampling ratio. As a quantitative measure of domain shift, we order target domains in decreasing order of their test accuracy under the pretrained source network, which generally corresponds well to human intuition of each task difficulty. We also draw inspiration from [3], which proposes to measure domain shift as the cosine distance between the mean responses in the before-to-last fully-connected layer of the source network applied to the source and target domain, denoted by $\cos_{\text{src}}$. We also report its per-class variant, $\cos_{\text{pc}}$.

Results. Quantitative results for all subsampling ratios and target domains are reported in Table 2, comparing flex-tuning and its variants to the fine-tuning baselines. As explained in the main paper, flex and fast-flex usually choose to fine-tune all layers (*i.e.* they recover ft-all), which achieves best accuracy out of the network-tuning method. While this is almost always the case in the full dataset scenarios, it happens less often in the small sample size settings, where there is a higher risk of overfitting when fine-tuning the whole network. Secondly, the overall best performing method is prep-tuning. In fact, the pre-processing module easily recovers from some domain shifts such as Blurry MNIST or Fixed Transformed MNIST, significantly improving the accuracies in these settings, especially in the small sample size scenarios.

In Table 3 and Figure 5, we report quantitative and qualitative results for the pre-processing module alone, without flex-tuning model selection. For the geometric transforms, we define this module as a Spatial Transformer Network [7] with a 1-layer encoder. Given an input image, the encoder outputs parameters for an affine transformation of the same form as the ones we considered for generating the shifted domains (*i.e.* a rescaling operations followed by a translation followed by a rotation). For the other, more generic, transformations, we consider a pix2pix architecture [6] taking inputs of size 32x32 pixels, with n layers in the encoder and n layers in the decoder (n ranging from 1 to 3). As mentioned in the original pix2pix paper, we tried using both upscaling + convolution and transpose convolutions. The latter usually yields slightly better classification accuracies but not by a significant margin and generates a lot of artifacts, hence we use the first method, which indeed generates more visually pleasing images. Finally we use standard batch normalization instead of instance normalization, as it did not significantly impact nor classification accuracies nor generated images in our experiments. As can be seen in these figures, when enough data is available, making use of all parameters in flex-prep (3) performs best. For smaller sample sizes, training a reduced number of parameters such as in flex-prep (2) is more advantageous.

MNIST		flex				ft-			
		flex	fast	faster	prep	fc (1)	fc (2)	ss	all
Blurry	(0.75)	0.890 ± 0.00	0.860 ± 0.00	0.857 ± 0.01	**0.950 ± 0.00**	0.867 ± 0.00	0.846 ± 0.01	0.862 ± 0.00	0.851 ± 0.00
Occluded	(0.58)	**0.695 ± 0.00**	0.664 ± 0.01	0.661 ± 0.01	**0.695 ± 0.00**	0.644 ± 0.01	0.654 ± 0.01	0.662 ± 0.00	0.660 ± 0.01
MNIST-M	(0.44)	0.564 ± 0.00	0.564 ± 0.00	0.528 ± 0.00	**0.643 ± 0.00**	0.524 ± 0.00	0.523 ± 0.01	0.540 ± 0.01	0.528 ± 0.00
SVHN	(0.21)	**0.426 ± 0.00**	**0.426 ± 0.00**	0.414 ± 0.00	**0.426 ± 0.00**	0.365 ± 0.01	0.412 ± 0.00	0.403 ± 0.00	**0.426 ± 0.00**
Transform (rnd)	(0.32)	0.400 ± 0.00	0.400 ± 0.00	0.399 ± 0.00	**0.498 ± 0.00**	0.391 ± 0.01	0.401 ± 0.00	0.395 ± 0.01	0.396 ± 0.00
Transform (fixed)	(0.16)	0.776 ± 0.00	0.776 ± 0.00	0.770 ± 0.00	**0.901 ± 0.00**	0.743 ± 0.00	0.768 ± 0.00	0.752 ± 0.00	0.776 ± 0.00

(a) Data subsampling ratio 0.001 ($\sim$ 3 images per class). Metrics are reported for 20 repetitions of the experiment with different sampled training images.

MNIST		flex				ft-			
		flex	fast	faster	prep	fc (1)	fc (2)	ss	all
Blurry	(0.75)	0.926	0.926	0.926	**0.957**	0.921	0.928	0.928	0.921
Occluded	(0.58)	**0.806**	**0.806**	0.801	**0.806**	0.785	0.801	0.792	**0.806**
MNIST-M	(0.44)	0.683	0.683	0.671	**0.776**	0.615	0.670	0.675	0.683
SVHN	(0.21)	**0.669**	**0.669**	0.572	**0.669**	0.451	0.595	0.657	**0.669**
Transform (rnd)	(0.32)	0.644	0.644	0.644	**0.666**	0.573	0.638	0.634	0.625
Transform (fixed)	(0.16)	0.908	0.887	0.879	**0.937**	0.839	0.875	0.866	0.887

(b) Data subsampling ratio 0.01 ($\sim$ 30 images per class).

MNIST		flex				ft-			
		flex	fast	faster	prep	fc (1)	fc (2)	ss	all
Blurry	(0.75)	0.967	0.967	0.967	**0.981**	0.941	0.964	0.957	0.965
Occluded	(0.58)	0.873	0.873	0.873	0.873	0.849	**0.875**	0.865	0.870
MNIST-M	(0.44)	0.828	0.828	0.795	**0.867**	0.704	0.797	0.783	0.828
SVHN	(0.21)	**0.849**	**0.849**	0.812	**0.849**	0.558	0.800	0.798	**0.849**
Transform (rnd)	(0.32)	**0.843**	**0.843**	0.830	**0.843**	0.683	0.836	0.760	**0.843**
Transform (fixed)	(0.16)	0.955	0.955	0.947	**0.973**	0.876	0.945	0.916	0.955

(c) Data subsampling ratio 0.1 ($\sim$ 300 images per class).

MNIST		flex				ft-			
		flex	fast	faster	prep	fc (1)	fc (2)	ss	all
Blurry	(0.75)	0.987	0.987	0.981	**0.988**	0.955	0.982	0.970	0.987
Occluded	(0.58)	**0.917**	**0.917**	0.915	**0.917**	0.867	0.912	0.893	**0.917**
MNIST-M	(0.44)	0.895	0.895	0.857	**0.953**	0.739	0.868	0.846	0.895
SVHN	(0.21)	**0.909**	**0.909**	0.851	**0.909**	0.670	0.877	0.848	**0.909**
Transform (rnd)	(0.32)	**0.941**	**0.941**	0.900	**0.941**	0.733	0.909	0.835	**0.941**
Transform (fixed)	(0.16)	0.979	0.979	0.963	**0.980**	0.900	0.969	0.943	0.979

(d) Experiments using the full target domain training dataset ($\sim$ 3000 images per class).

Table 2: Quantitative results for the MNIST source domain. We report on experiments with the proposed *flex-tuning* (`flex`), its two faster variants *fast flex-tuning* (`fast-flex`) and *even faster flex-tuning* (`faster-flex`), as well as flex-tuning augmented with a *preprocessing module* (`flex-prep`). We compare against transfer learning baselines: fine-tuning *all layers* in the architecture (`ft-all`), versus fine-tuning only *fully-connected* ones, either only the last one (`ft-fc` (1)) or both of them (`ft-fc` (2)), and finally adding scale and shift operations (`ft-ss`).

MNIST	Ratio 0.001			Ratio 0.010			Ratio 0.100			Ratio 1.000		
	prep (3)	prep (2)	prep (1)	prep (3)	prep (2)	prep (1)	prep (3)	prep (2)	prep (1)	prep (3)	prep (2)	prep (1)
Blurry	0.817	**0.950**	0.917	0.939	**0.957**	0.955	0.974	**0.981**	0.967	0.987	**0.988**	0.975
Occluded	0.452	**0.536**	0.504	0.686	**0.703**	0.646	0.828	**0.830**	0.729	**0.903**	0.897	0.791
MNIST-M	0.410	0.630	**0.643**	0.638	**0.776**	0.725	0.840	**0.867**	0.843	**0.953**	0.949	0.865
SVHN	0.227	**0.261**	0.244	**0.476**	0.418	0.369	**0.752**	0.664	0.431	**0.881**	0.833	0.469
Transform (rnd)	**0.498**	-	-	**0.666**	-	-	**0.826**	-	-	**0.924**	-	-
Transform (fixed)	**0.901**	-	-	**0.937**	-	-	**0.973**	-	-	**0.980**	-	-

Table 3: Quantitative results from the pre-processing module experiments for different architectures and subsampling ratio For the pix2pix network, `prep` (n) designates an architecture with n layers in the encoder and n layers in the decoder.

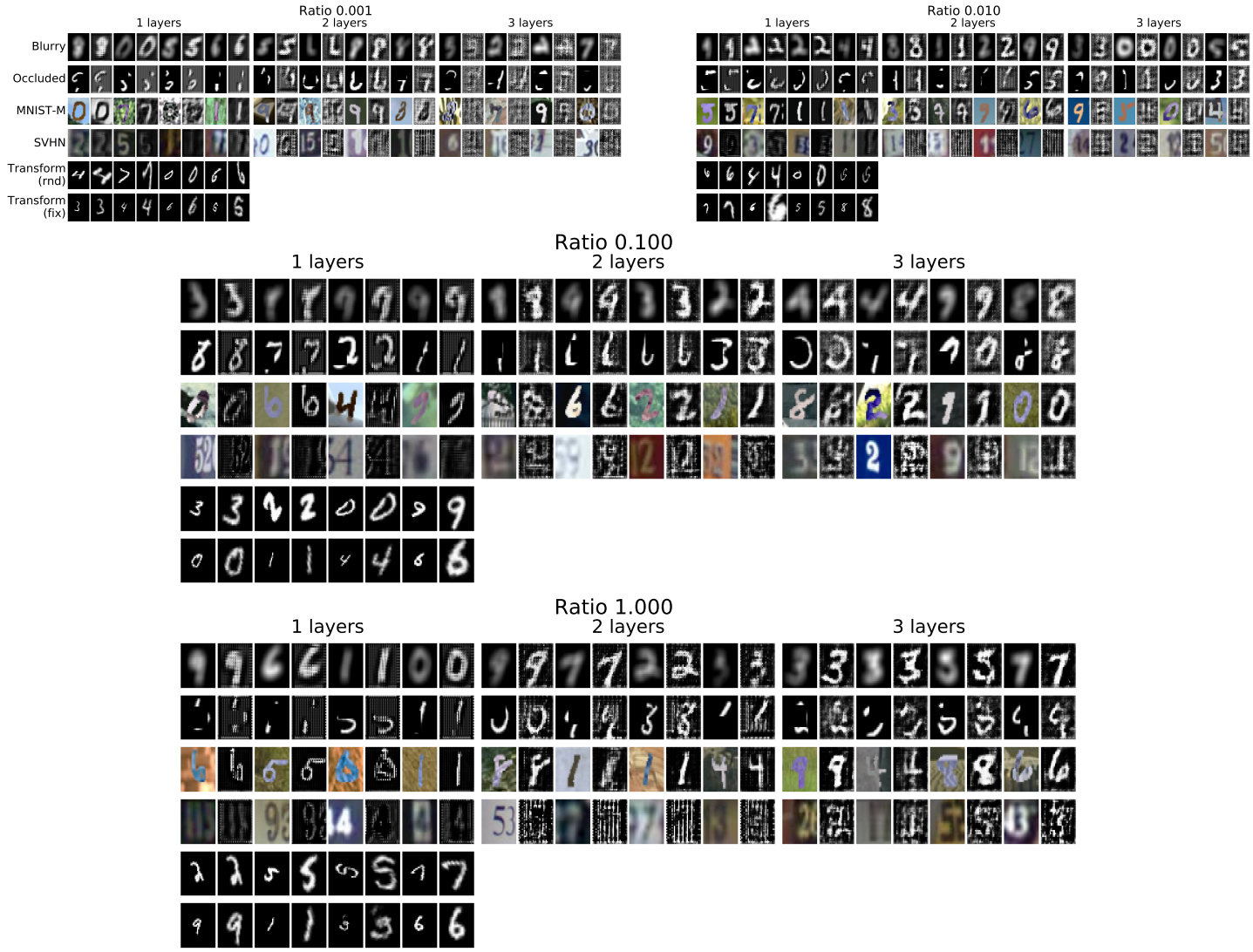

Figure 5: Qualitative results obtained with the pre-processing module for each subsampling ratio, target domain and pre-processing module architecture. Figures reads row-wise, two-by-two, where each pair contains the input image on the left (target domain) and the generated pre-processed image on the right (source domain). Best seen in PDF with zoom.

3. CIFAR and Quick, Draw! experiments

Datasets and base architecture. We experiment on a standard middle-sized architecture composed of 5 convolutional layers followed by 2 fully-connected ones. Each layer is equipped with ReLU activations, except for the last one, and each convolutional layer is followed by max-pooling. We consider as source domains the CIFAR-10 [8] and Quick, Draw! [1] datasets. As we will use each of them as target domain for the other, we restrict ourselves to classes they have in common, *i.e*. all CIFAR classes except one: "airplane", "automobile", "bird", "cat", "dog", "frog", "horse", "ship" and "truck".

For **CIFAR**, we first randomly split the training set in two. We use the first split, containing 17991 images, to pre-train the network. The final model reaches **0.738** top-1 accuracy on the test set. We further divide the remaining split in two: A training set of 18006 images, $\mathcal{D}_{\text{train}}$, which we use to generate synthetic domain shifts, and a validation set, $\mathcal{D}_{\text{val}}$, of size 9003. We use the original test split of CIFAR containing 9000 images for testing purposes.

For the **Quick, Draw!** dataset, we first extract 10000 random images from each of the nine categories of interest and resize them to size 32x32 pixels: using the full original dataset of 50 million images would create a huge discrepancy in terms of dataset size. We again split this set of images into 40000 image to pre-train the source model on Quick, Draw!, reaching **0.654** top-1 test accuracy, a set of 30000 images, $\mathcal{D}_{\text{train}}$, that we use for creating synthetic target domain training sets, a set of 5000 images used for validation purposes, $\mathcal{D}_{\text{val}}$, and finally the remaining 15000 images we use as our test split, $\mathcal{D}_{\text{test}}$.

Starting from CIFAR as a source domain, we then create the following target domains: To obtain **Blurry CIFAR**, we apply a Gaussian blur with a kernel of length 4 and standard deviation $\sigma = 0.5$ on all images in $\mathcal{D} = (\mathcal{D}_{\text{train}}, \mathcal{D}_{\text{val}}, \mathcal{D}_{\text{test}})$. Similarly, we create **Noisy CIFAR** by adding random-generated Gaussian noise with mean 0 and standard deviation 30 (images ranging in [0, 255]) to each image in $\mathcal{D}$. Note that the transformation is done once so that the dataset is the same for all settings. Finally, we create a **Quick, Draw!** target domain by simply using the $\mathcal{D}_{\text{train}}$, $\mathcal{D}_{\text{val}}$ and $\mathcal{D}_{\text{test}}$ for the Quick, Draw! dataset as defined in the previous paragraph. For the Quick, Draw! dataset as the source domain, we define target domains **Blurry QuickDraw**, **Noisy QuickDraw** and **CIFAR** in the same manner.

As for the MNIST experiments, we also create subsampled versions of each target training dataset, $\mathcal{D}_{\text{train}}$, by randomly sampling images with ratios 0.001, 0.01 and 0.1. A summary of our experimental setup is given in Table 4.

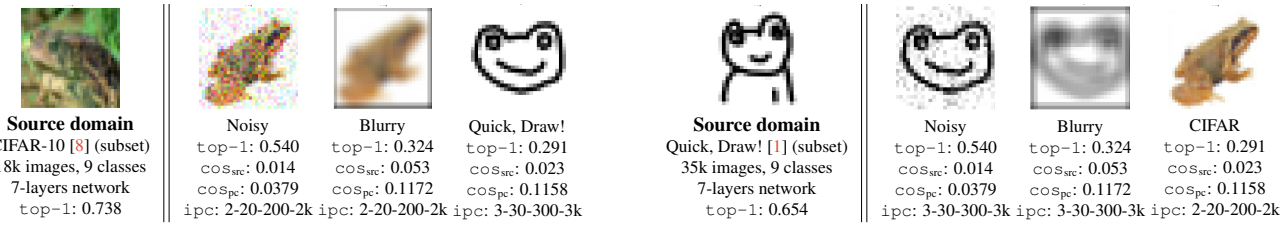

Table 4: CIFAR (left) and Quick, Draw! (right) based domain shifts we consider in our experimental setup.

Results. Quantitative results for all subsampling ratios and target domains are reported in Table 5 for experiments using CIFAR as their source domain, and in Table 6 for experiments with Quick, Draw! as the source domain. As in Section 2, we observe that in the full dataset scenario, fine-tuning all layers yields best performance, and is indeed chosen by flex-tuning and fast flex-tuning. As the sample size decreases, this is however not always true and a few settings benefit from fine-tuning a specific unit in the network instead.

In Table 7, Figure 7 and Figure 6, we report quantitative and qualitative results for the pre-processing module experiment. We use the same Pix2Pix network as described in Section 2. We observe that the pre-processing module performs well for the scenarios with Quick, Draw! as their source domain, most likely due to the simple appearance of this domain. In the other, more complex, settings, it fails to nicely recover the source CIFAR domain, even when the full dataset is available, which leads to poor classification accuracies.

CIFAR	flex				ft-			
	flex	fast	faster	prep	fc (1)	fc (2)	ss	all
Blurry (0.32)	**0.514 ± 0.00**	**0.514 ± 0.00**	0.344 ± 0.02	**0.514 ± 0.00**	0.408 ± 0.00	0.427 ± 0.00	0.490 ± 0.00	0.476 ± 0.01
Noisy (0.54)	**0.618 ± 0.00**	0.618 ± 0.00	0.618 ± 0.00	**0.618 ± 0.00**	0.555 ± 0.00	0.566 ± 0.00	0.603 ± 0.01	0.582 ± 0.00
QuickDraw (0.29)	**0.392 ± 0.00**	0.391 ± 0.00	0.386 ± 0.00	**0.392 ± 0.00**	0.359 ± 0.00	0.380 ± 0.01	0.378 ± 0.01	0.391 ± 0.00

(a) Data subsampling ratio 0.001 ($\sim$ 2 images per class). Metrics are reported for 20 repetitions of the experiment with different sampled training images.

CIFAR	flex				ft-			
	flex	fast	faster	prep	fc (1)	fc (2)	ss	all
Blurry (0.32)	**0.577**	**0.577**	0.512	**0.577**	0.444	0.501	0.569	**0.577**
Noisy (0.54)	**0.624**	**0.624**	**0.624**	**0.624**	0.583	0.597	0.618	0.621
QuickDraw (0.29)	0.518	0.517	0.517	0.518	0.475	**0.525**	0.495	0.501

(b) Data subsampling ratio 0.01 ($\sim$ 20 images per class).

CIFAR	flex				ft-			
	flex	fast	faster	prep	fc (1)	fc (2)	ss	all
Blurry (0.32)	0.609	0.608	0.566	0.609	0.525	0.552	**0.623**	0.608
Noisy (0.54)	0.644	0.629	0.629	0.644	0.602	0.620	**0.653**	0.613
QuickDraw (0.29)	0.663	0.667	0.667	0.663	0.569	0.662	0.643	**0.671**

(c) Data subsampling ratio 0.01 ($\sim$ 200 images per class).

CIFAR	flex				ft-			
	flex	fast	faster	prep	fc (1)	fc (2)	ss	all
Blurry (0.32)	**0.689**	**0.689**	0.644	**0.689**	0.560	0.609	0.685	**0.689**
Noisy (0.54)	0.685	0.685	0.651	0.685	0.633	0.640	**0.705**	0.685
QuickDraw (0.29)	**0.786**	**0.786**	0.744	**0.786**	0.581	0.721	0.702	**0.786**

(d) Experiments using the full target domain training dataset ($\sim$ 3000 images per class).

Table 5: Quantitative results for the CIFAR source domain. We report on experiments with the proposed *flex-tuning* (`flex`), its two faster variants *fast flex-tuning* (`fast-flex`) and *even faster flex-tuning* (`faster-flex`), as well as flex-tuning augmented with a *preprocessing module* (`flex-prep`). We compare against transfer learning baselines: fine-tuning *all layers* in the architecture (`ft-all`), versus fine-tuning only *fully-connected* ones, either only the last one (`ft-fc` (1)) or both of them (`ft-fc` (2)).

QuickDraw	flex				ft-			
	flex	fast	faster	prep	fc (1)	fc (2)	ss	all
Blurry (0.19)	**0.560 ± 0.01**	**0.560 ± 0.01**	0.525 ± 0.00	**0.560 ± 0.01**	0.290 ± 0.00	0.325 ± 0.00	0.327 ± 0.00	0.386 ± 0.00
Noisy (0.63)	0.763 ± 0.00	0.760 ± 0.00	0.758 ± 0.00	0.763 ± 0.00	0.766 ± 0.00	0.768 ± 0.00	**0.782 ± 0.01**	0.757 ± 0.01
CIFAR (0.20)	0.241 ± 0.00	0.241 ± 0.00	0.230 ± 0.00	0.241 ± 0.00	0.203 ± 0.00	0.228 ± 0.00	**0.264 ± 0.01**	0.241 ± 0.00

(a) Data subsampling ratio 0.001 ($\sim$ 2 images per class). Metrics are reported for 20 repetitions of the experiment with different sampled training images.

QuickDraw	flex				ft-			
	flex	fast	faster	prep	fc (1)	fc (2)	ss	all
Blurry (0.19)	0.642	0.631	0.560	**0.642**	0.426	0.468	**0.707**	0.631
Noisy (0.63)	0.801	0.801	0.795	0.801	0.788	0.792	**0.805**	0.801
CIFAR (0.20)	**0.424**	**0.424**	0.401	**0.424**	0.333	0.347	0.388	**0.424**

(b) Data subsampling ratio 0.01 ($\sim$ 20 images per class).

QuickDraw	flex				ft-			
	flex	fast	faster	prep	fc (1)	fc (2)	ss	all
Blurry (0.19)	**0.726**	0.722	0.595	**0.726**	0.471	0.583	0.724	0.722
Noisy (0.63)	**0.815**	0.797	0.797	**0.815**	**0.815**	0.797	0.812	0.772
CIFAR (0.20)	**0.601**	**0.601**	0.532	**0.601**	0.394	0.413	0.543	**0.601**

(c) Data subsampling ratio 0.01 ($\sim$ 200 images per class).

QuickDraw	flex				ft-			
	flex	fast	faster	prep	fc (1)	fc (2)	ss	all
Blurry (0.19)	**0.776**	**0.776**	0.613	**0.776**	0.453	0.629	0.658	**0.776**
Noisy (0.63)	0.817	**0.822**	**0.822**	0.817	0.789	0.818	0.814	0.794
CIFAR (0.20)	**0.718**	**0.718**	0.632	**0.718**	0.432	0.529	0.697	**0.718**

(d) Experiments using the full target domain training dataset ($\sim$ 3000 images per class).

Table 6: Quantitative results for the Quick, Draw! source domain. We report on experiments with the proposed *flex-tuning* (`flex`), its two faster variants *fast flex-tuning* (`fast-flex`) and *even faster flex-tuning* (`faster-flex`), as well as flex-tuning augmented with a *preprocessing module* (`flex-prep`). We compare against transfer learning baselines: fine-tuning *all layers* in the architecture (`ft-all`), versus fine-tuning only *fully-connected* ones, either only the last one (`ft-fc` (1)) or both of them (`ft-fc` (2)).

CIFAR	Ratio 0.001			Ratio 0.010			Ratio 0.100			Ratio 1.000		
	prep (3)	prep (2)	prep (1)	prep (3)	prep (2)	prep (1)	prep (3)	prep (2)	prep (1)	prep (3)	prep (2)	prep (1)
Blurry	0.123	0.165	**0.184**	0.147	**0.283**	0.246	**0.433**	0.342	0.341	**0.598**	0.568	0.382
Noisy	0.118	0.164	**0.176**	**0.228**	0.206	0.210	0.408	0.279	**0.463**	**0.552**	0.498	0.534
QuickDraw	0.227	0.216	**0.256**	**0.421**	0.400	0.264	**0.596**	0.548	0.435	**0.764**	0.722	0.449

QuickDraw	Ratio 0.001			Ratio 0.010			Ratio 0.100			Ratio 1.000		
	prep (3)	prep (2)	prep (1)	prep (3)	prep (2)	prep (1)	prep (3)	prep (2)	prep (1)	prep (3)	prep (2)	prep (1)
Blurry	0.285	0.338	**0.523**	0.458	0.550	**0.571**	0.633	**0.639**	0.618	**0.722**	0.691	0.646
Noisy	0.330	0.415	**0.537**	0.579	0.537	**0.585**	**0.651**	0.622	0.635	**0.739**	0.714	0.652
CIFAR	0.140	0.125	**0.167**	**0.219**	0.175	0.207	**0.410**	0.309	0.265	**0.622**	0.437	0.305

Table 7: Quantitative results for the pre-processing module experiments on CIFAR and Quick, Draw! source domains

Figure 6: Qualitative results from the pre-processing module experiments with CIFAR as the source domain.

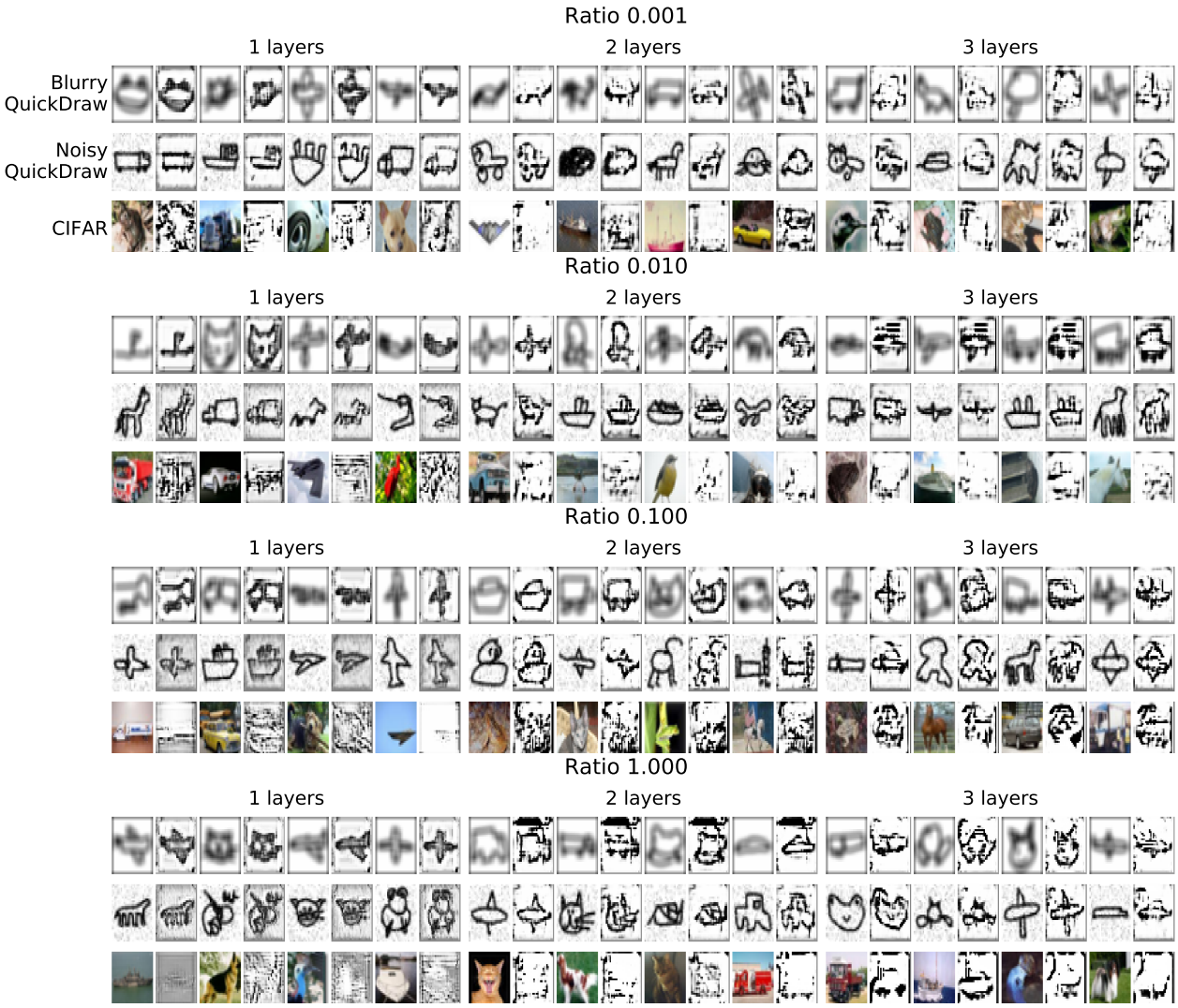

Figure 7: Qualitative results from the pre-processing module experiments with Quick, Draw! as the source domain.

4. ILSVRC experiments

Datasets and base architecture. For this setting, we employ a standard Inception2 architecture, pre-trained on the ILSVRC12 train split, and implemented in the tensornets framework [14]. This source pre-trained network reaches **0.918** top-5 accuracy on the test set. For all experimental settings, we also follow the same pre-processing as used for the original network: we resize all images to 256x256 pixels and feed the network with central crop of size 224x224px.

To generate target domains, we first split the ILSVRC12 validation split into three random sets: 25k images for training, $\mathcal{D}_{\text{train}}$, 5k images for validation, $\mathcal{D}_{\text{val}}$, and finally 20k images for testing purposes, $\mathcal{D}_{\text{test}}$. We first generate **YUV ILSVRC** and **HSV ILSVRC** by converting all images from $\mathcal{D} = (\mathcal{D}_{\text{train}}, \mathcal{D}_{\text{val}}, \mathcal{D}_{\text{test}})$ from RGB to YUV and HSV color spaces, respectively. We then generate three geometric transformed target domains: **Fixed Scaling (stretch)** is obtained by rescaling all images with the same fixed coefficient $s = 0.5$ and padding the empty pixels by repeating the edges values of the images. **Fixed Scaling (symmetric)** is obtained similarly but using the SYMMETRIC padding mode of TensorFlow. Finally, **Fixed Rotation** corresponds to applying the same fixed rotation with angle 0.6 radians to all images.

We also create subsampled versions of each target training dataset by randomly sampling images with ratios 0.04 ($\sim$ 1 image per class) and 0.5 ($\sim$ 12 images per class). A summary of our experimental setup is given in Table 8.

	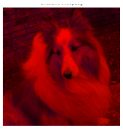				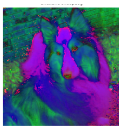
Source domain **ILSVRC** [13] **('12 train split)** 1M images, 1000 classes Inception2 top-5: 0.918	YUV top-5: 0.841 $\cos_{\text{src}}$: 0.0231 $\cos_{\text{pc}}$: 0.079 ipc: 2 - 12 - 25	Fixed rotation top-5: 0.743 $\cos_{\text{src}}$: 0.0104 $\cos_{\text{pc}}$: 0.096 ipc: 2 - 12 - 25	Fixed scaling (symmetric) top-5: 0.519 $\cos_{\text{src}}$: 0.0644 $\cos_{\text{pc}}$: 0.187 ipc: 2 - 12 - 25	Fixed scaling (stretch) top-5: 0.440 $\cos_{\text{src}}$: 0.0861 $\cos_{\text{pc}}$: 0.216 ipc: 2 - 12 - 25	HSV top-5: 0.384 $\cos_{\text{src}}$: 0.0787 $\cos_{\text{pc}}$: 0.225 ipc: 2 - 12 - 25

Table 8: ILSVRC-based domain shifts we consider in our experimental setup.

Results. Quantitative results for all subsampling ratios and target domains are reported in Table 9, comparing flex-tuning and its variants to the fine-tuning baselines. In all settings, fine-tuning all layers performs badly as the network tends to overfit due to the rather small sample sizes. Furthermore, flex-tuning and its variants consistently outperform the other fine-tuning baseline, `ft-fc`. In the YUV and HSV settings, all three flex-tuning variants perform similarly as they indeed pick the same unit to fine-tune (second or third convolutional layer). The unit choice is not as consistent for the geometric transformations, but the actual classification accuracies are also similar for all flex-tuning variants.

Moreover, we observe that the best performing method is prep-tuning (*i.e.*, flex-tuning augmented with a pre-processng module). In fact, as was the case in Section 2, the specialized pre-processing modules performs very well to recover the original source domain on these transformations, even in the small sample size setting. This can also be observed in Table 10 and Figure 8, in whic we report quantitative and qualitative results for the pre-processing module experiments. For geometric transforms, we use a Spatial Transformer Network as described in Section 2, this time with a 4-layers encoder that takes as input 224x224 images. For color channel conversions, we use a simple network composed only of 1x1 convolutions, either with only one layer, which is enough to model linear relations such as RGB $\rightarrow$ YUV, or with 2 layers and tanh activation in-between for the more complex RGB $\rightarrow$ HSV transformation.

ILSVRC	flex				ft-		
	flex	fast	faster	prep	fc	ss	all
YUV (0.84)	0.856 ± 0.00	0.857 ± 0.00	0.830 ± 0.00	**0.902 ± 0.00**	0.775 ± 0.00	0.574 ± 0.00	0.817 ± 0.00
HSV (0.38)	0.750 ± 0.01	0.750 ± 0.01	0.750 ± 0.01	**0.895 ± 0.00**	0.422 ± 0.01	0.374 ± 0.01	0.582 ± 0.00
Scaling (stretch) (0.44)	0.626 ± 0.01	0.612 ± 0.02	0.596 ± 0.00	**0.780 ± 0.00**	0.361 ± 0.01	0.425 ± 0.00	0.595 ± 0.01
Scaling (sym.) (0.52)	0.703 ± 0.01	0.700 ± 0.00	0.700 ± 0.00	**0.837 ± 0.00**	0.531 ± 0.00	0.525 ± 0.00	0.659 ± 0.00
Rotation (0.74)	0.771 ± 0.00	0.769 ± 0.01	0.750 ± 0.01	**0.837 ± 0.00**	0.621 ± 0.00	0.499 ± 0.01	0.718 ± 0.00

(a) Data subsampling ratio 0.04 (∼ 1 image per class). Metrics are reported for 20 repetitions of the experiment with different sampled training images.

ILSVRC	flex				ft-		
	flex	fast	faster	prep	fc	ss	all
YUV (0.84)	0.893	0.893	0.893	**0.903**	0.835	0.699	0.808
HSV (0.38)	0.856	0.856	0.856	**0.905**	0.533	0.646	0.687
Scaling (stretch) (0.44)	0.724	0.696	0.696	**0.803**	0.502	0.584	0.653
Scaling (sym.) (0.52)	0.770	0.757	0.757	**0.856**	0.663	0.650	0.716
Rotation (0.74)	0.826	**0.832**	0.812	0.826	0.667	0.652	0.771

(b) Data subsampling ratio 0.5 (∼ 12 images per class).

ILSVRC	flex				ft-		
	flex	fast	faster	prep	fc	ss	all
YUV (0.84)	0.897	0.897	0.897	**0.903**	0.839	0.716	0.818
HSV (0.38)	0.863	0.863	0.863	**0.904**	0.545	0.676	0.670
Scaling (stretch) (0.44)	0.750	0.706	0.706	**0.778**	0.515	0.597	0.675
Scaling (sym.) (0.52)	0.787	0.770	0.770	**0.880**	0.668	0.655	0.728
Rotation (0.74)	**0.837**	0.829	0.812	**0.837**	0.674	0.663	0.764

(c) Experiments using the full target domain training dataset (∼ 25 images per class).

Table 9: Quantitative results for the ILSVRC12 source domain. We report on experiments with the proposed *flex-tuning* (`flex`), its two faster variants *fast flex-tuning* (`fast-flex`) and *even faster flex-tuning* (`faster-flex`), as well as flex-tuning augmented with a *preprocessing module* (`flex-prep`). We compare against transfer learning baselines: fine-tuning *all layers* in the architecture (`ft-all`), versus fine-tuning only the single last *fully-connected* layer (`ft-fc`).

ILSVRC	Ratio 0.010		Ratio 0.500		Ratio 1.000	
	prep (1)	prep (2)	prep (1)	prep (2)	prep (1)	prep (2)
YUV	**0.902**	0.901	**0.903**	0.711	**0.903**	**0.903**
HSV	**0.895**	0.686	0.896	**0.905**	0.895	**0.904**
Scaling (stretch)	**0.780**	-	**0.803**	-	**0.778**	-
Scaling (sym.)	**0.837**	-	**0.856**	-	**0.880**	-
Rotation	**0.837**	-	**0.826**	-	**0.831**	-

Table 10: Quantitative results from the pre-processing module experiments for different architectures. For the color channel experiments, `prep` (n) designates a pre-processing architecture with n 1x1 convolutional layers.

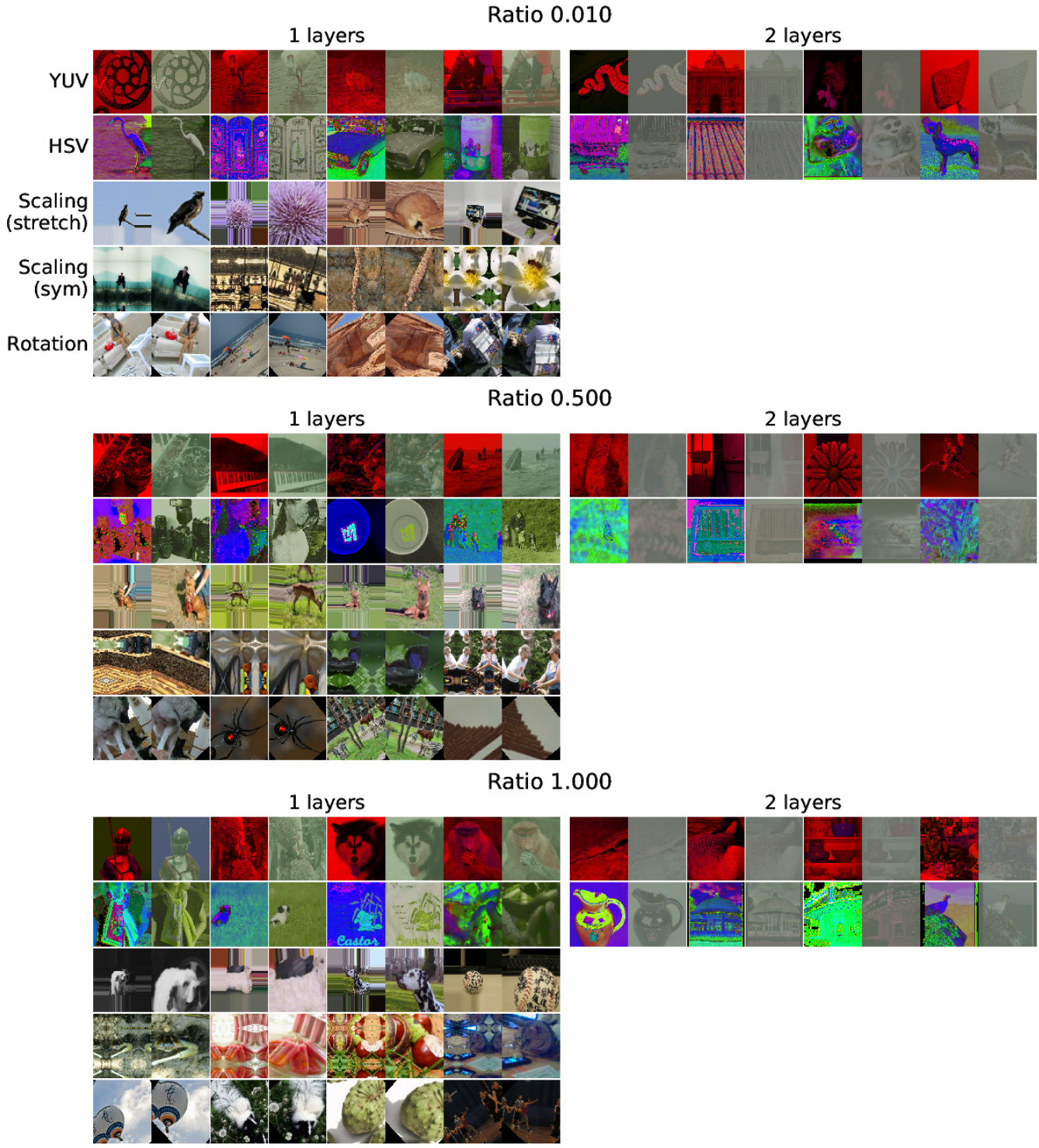

Figure 8: Qualitative results from the pre-processing module for each subsampling ratio, target domain and pre-processing module architecture. Figures read row-wise, two-by-two, where each pair contains the input image on the left (target domain) and the generated pre-processed image on the right (source domain). Best seen in PDF with zoom.

5. PACS Experiments

Datasets and base architecture. Our most challenging setting is based of the PACS dataset [10], initially introduced for domain generalization. The dataset contains 7 object categories, with occurences in 4 different artistic styles. We first randomly split each artistic style in a training, validation and test set. We then use a pre-trained ILSVRC12-pretrained Inception2 network as our base source model. We map PACS classes to the closest category in the ILSVRC classification task, and ignore the class "person" as it does not have any satisfying equivalent. For reference, even though it was not trained on it, it reaches top-1 accuracy of **0.885** on the test set for the **photo** split of PACS. We use the remaining artistic styles, **artistic paintings**, **cartoon** and **sketch** as our target domains.

			
Source domain	PACS (art)	PACS (cartoon)	PACS (sketch)
ILSVRC [13]	`top-1`: 0.532	`top-1`: 0.346	`top-1`: 0.142
1M images, 1000 classes	$\texttt{cos}_{\text{src}}$: 0.061	$\texttt{cos}_{\text{src}}$: 0.1361	$\texttt{cos}_{\text{src}}$: 0.211
Inception2	$\texttt{cos}_{\text{pc}}$: 0.090	$\texttt{cos}_{\text{pc}}$: 0.189	$\texttt{cos}_{\text{pc}}$: 0.257
`top-5`: 0.918	`ipc`: 2-20-200	`ipc`: 2-20-200	`ipc`: 4-40-400

Table 11: PACS-based domain shifts we consider in our experimental setup.

As for other datasets, we also create subsampled versions of each target training dataset by randomly sampling images with ratios 0.01, 0.1 and 1.0. A summary of our experimental setup is given in Table 11.

Results. Quantitative results comparing `flex` and variants to the fine-tuning baselines for all subsampling ratios and target domains are reported in the main paper. As for the ILSVRC setting, `ft-all` is very prone to overfitting and usually performs badly. Out of the other methods, `flex` and variants yields better performance than the other fine-tuning baseline, `ft-fc`, showing that there is benefit to selecting the best unit to tune.

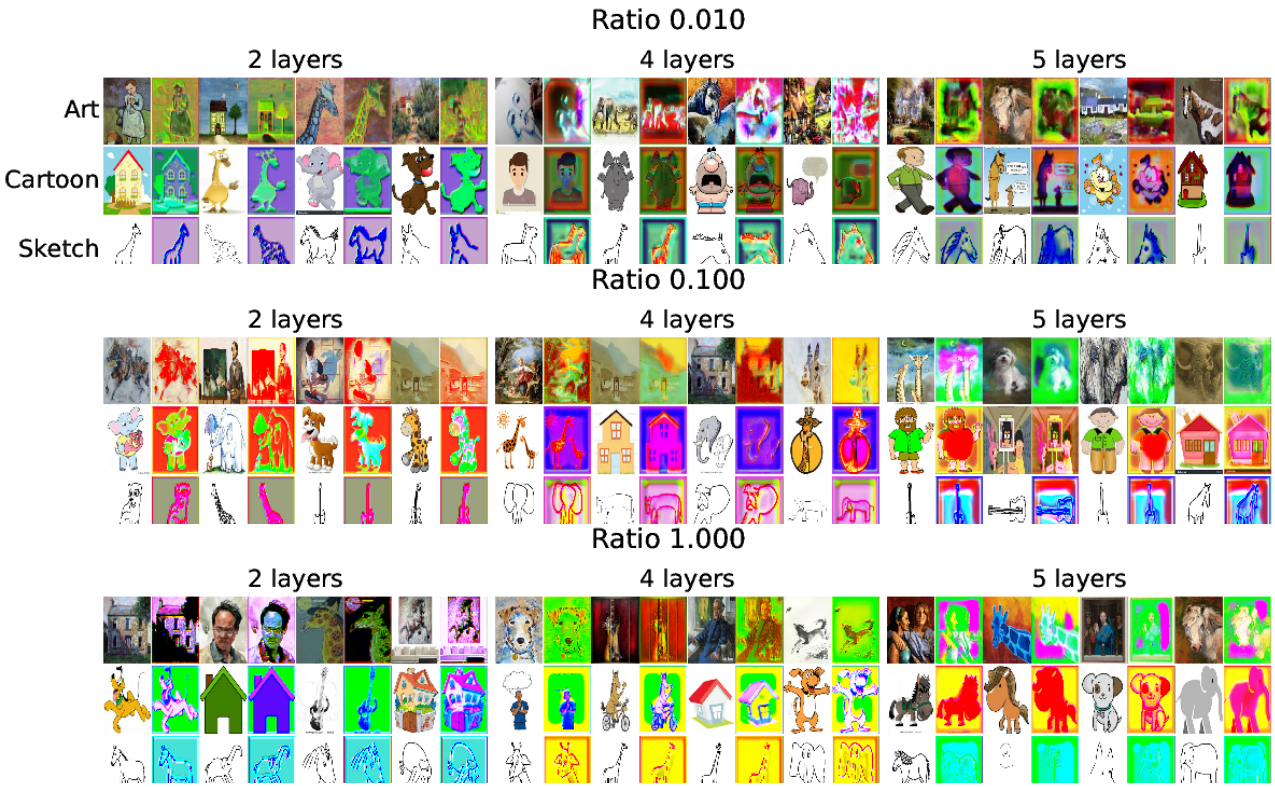

Figure 9: Qualitative results from the pre-processing module for PACS experiments.

Secondly, we note that in this scenario, the pre-processing module performs very badly and does not help flex-tuning. In fact, with these widely different artistic styles, the image-to-image translation problem becomes significantly harder than the classification task we actually want to solve. In consequence, prep-tuning always reduces to flex-tuning in that scenario.

This can also be seen in Table 12 and Figure 9, in which we report quantitative and qualitative results for the pre-processing module experiments. We used pix2pix as described in Section 2 with increased depth to match the larger input size.

ILSVRC	Ratio 0.010			Ratio 0.100			Ratio 1.000		
	prep (5)	prep (4)	prep (2)	prep (5)	prep (4)	prep (2)	prep (5)	prep (4)	prep (2)
Art	**0.365**	0.331	0.343	**0.504**	0.451	0.472	0.482	0.513	**0.568**
Cartoon	0.333	**0.369**	0.358	**0.493**	0.335	0.447	0.470	0.606	**0.633**
Sketch	0.361	0.354	**0.390**	**0.636**	0.422	0.286	0.551	0.531	**0.594**

Table 12: Quantitative results from the pre-processing module for PACS experiments. For the pix2pix network, `prep` (n) designates an architecture with n layers in the encoder and n layers in the decoder.

6. Retrieval Experiments

In this set of experiments, we assess how much the representations learned by the tuned network differ from the initial representations from the source network on the source domain: Since the target domain visually differs from the source, extracting features from the pretrained source network directly, e.g. as is done with fine-tuning, leads to misaligned representations. While tuning intermediate units could help "mend" the representations and recovering an embedding space close to that of the original source network. To evaluate this, we use the following retrieval experiment: We extract features for the initial source validation domain through the source network, as well as for the target domain through the flextuned (best intermediate unit according to validation accuracy) or finetuned network. For each target sample, we then retrieve its top-k nearest neighbors in the source domain and consider them correctly retrieved if they share the same semantic class, and evaluate the average precision (AP@k). we report AP@1, AP@10, and AP@100 for our main experimental settings in Table 13. Qualitative results are also available in Figure 10 to Figure 13 .

The results follow the same global observations as other experiments: **(i)** Fine-tuning the last fully-connected layer is enough to learn a classifier but can not modify the feature extract part of the network, hence low retrieval results; **(ii)** allowing to tune intermediate units often recover representations close to the one of the source embedding. In particular, when the target domain differ from the source domain at a very low-level (e.g., color channels or noise), then targetting a single unit such as in flex-tuning usually yields better results. For the other domain shifts, it seems that flex-tuning is usually a better alternative on larger architectures, while for smaller architectures, fine-tuning all layers yield the best results.

Source	MNIST				CIFAR			ILSVRC		PACS		
Target	Blurry	Occl.	-M	SVHN	Blurry	Noisy	QDraw	YUV	HSV	Art	Cartoon	Sketch
`ft-fc`	0.32	0.67	0.44	0.15	0.27	0.55	0.23	0.86	0.45	0.62	0.45	0.35
`ft-all`	**0.91**	**0.84**	**0.74**	**0.58**	**0.58**	0.58	**0.65**	0.79	0.48	0.82	0.81	0.87
`flex`	0.73	0.80	0.57	0.34	0.44	**0.63**	0.45	**0.94**	**0.95**	**0.90**	**0.84**	**0.90**

a) AP@1 results

Source	MNIST				CIFAR			ILSVRC		PACS		
Target	Blurry	Occl.	-M	SVHN	Blurry	Noisy	QDraw	YUV	HSV	Art	Cartoon	Sketch
`ft-fc`	0.38	0.70	0.47	0.19	0.36	0.58	0.27	0.80	0.47	0.66	0.53	0.39
`ft-all`	**0.91**	**0.85**	**0.76**	**0.63**	**0.64**	0.64	**0.69**	0.75	0.52	0.80	0.83	0.85
`flex`	0.76	0.83	0.61	0.40	0.52	**0.67**	0.54	**0.85**	**0.85**	**0.88**	**0.86**	**0.86**

b) AP@10 results

Source	MNIST				CIFAR			ILSVRC		PACS		
Target	Blurry	Occl.	-M	SVHN	Blurry	Noisy	QDraw	YUV	HSV	Art	Cartoon	Sketch
`ft-fc`	0.28	0.61	0.41	0.16	0.28	0.47	0.24	0.66	0.39	0.50	0.42	0.27
`ft-all`	**0.82**	**0.80**	**0.70**	**0.54**	**0.55**	0.53	**0.63**	0.61	0.42	0.65	0.70	0.66
`flex`	0.61	0.76	0.53	0.32	0.37	**0.56**	0.43	**0.71**	**0.72**	**0.75**	**0.74**	**0.71**

c) AP@100 results

Table 13: mAP retrieval results for the fine– and flex-tuned network embeddings of the target domain (second row), queried against the source domain embeddings (first row)

Figure 10: Qualitative Results for retrieval experiments on MNIST. First column contains the query from the target domain. Next groups of columns contains the ten closest samples from the source domain, when using the target embeddings from `flex`, `ft-fc` and `ft-all` respectively

Figure 11: Qualitative Results for retrieval experiments on CIFAR.

Figure 12: Qualitative Results for retrieval experiments on PACS.

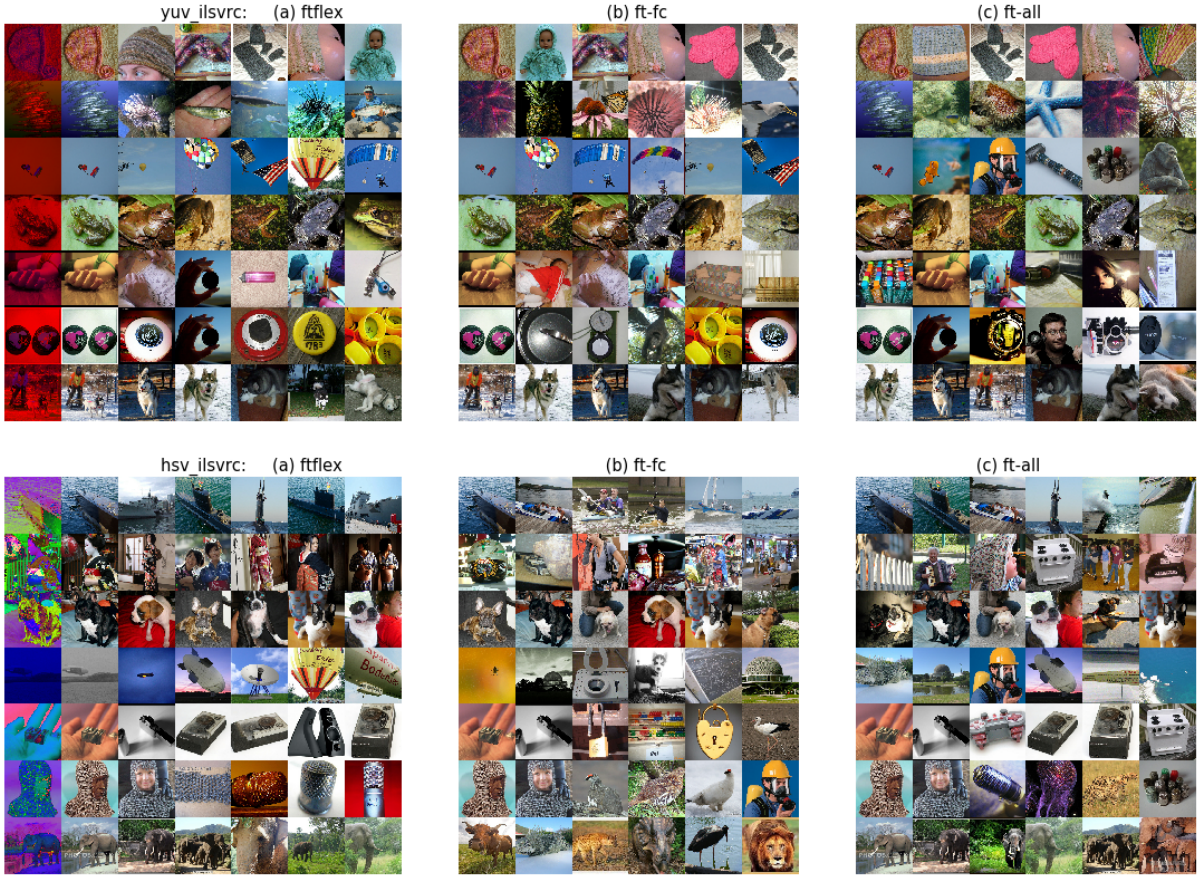

Figure 13: Qualitative Results for retrieval experiments on Colorized-ILSVRC.

7. Results for cosine classifiers

Finally in this section we report results for an additional transfer learning baseline inspired from [2]. It consists in applying fine-tuning on a neural network where the standard last linear classification layer is replaced by a cosine classifier, providing additional feature normalization. Note that we did not experiment on our ILSVRC-based settings as these would have required retraining the source network on ILSVRC's full training set. Nonetheless, in Table 14 we report results on the remaining setting and observe that (i) the base accuracy of the network trained with a cosine classifier is often slightly worse than the one trained without (see numbers in parenthesis in the first column) and (ii) this baseline performs much worse than simply finetuning a standard linear classification layer. A possible explanation is that since the method still only acts on the last layer, it is not enough to handle important visual dissimilarities at the input level. In particular, it aims to learn good "prototypes" in the feature space to describe each class, and in fact this method was rather intended to tackle different settings from ours: where the input domains are similar and semantic classes are different: Hence the feature representations of both domains lie in a similar subspace and only the prototypes have to be relearned for the new semantic classes.

	0.001 ratio		0.01 ratio		0.1 ratio		full	
	ft-fc	ft-cosine	ft-fc	ft-cosine	ft-fc	ft-cosine	ft-fc	ft-cosine
Blurry (0.63)	0.867	0.656	0.921	0.690	0.941	0.696	0.955	0.706
Occluded (0.58)	0.644	0.563	0.785	0.582	0.849	0.586	0.867	0.585
MNIST-M (0.35)	0.524	0.463	0.615	0.462	0.704	0.477	0.739	0.479
SVHN (0.20)	0.365	0.297	0.451	0.321	0.558	0.339	0.670	0.342

	0.001 ratio		0.01 ratio		0.1 ratio		full	
	ft-fc	ft-cosine	ft-fc	ft-cosine	ft-fc	ft-cosine	ft-fc	ft-cosine
Blurry (0.32)	0.408	0.253	0.444	0.334	0.525	0.338	0.560	0.341
Noisy (0.57)	0.555	0.508	0.583	0.585	0.602	0.586	0.633	0.586
QuickDraw (0.31)	0.359	0.259	0.475	0.308	0.569	0.315	0.581	0.390

Table 14: Results of the baseline using cosine classifiers similar to [2] on the MNIST and CIFAR settings

References

[1] S. Cheema, S. Gulwani, and J. LaViola. QuickDraw: Improving drawing experience for geometric diagrams. In *Conference on Human Factors in Computing Systems (SIGCHI)*, 2012.

[2] W.-Y. Chen, Y.-C. Liu, Z. Kira, Y.-C. F. Wang, and J.-B. Huang. A closer look at few-shot classification. In *International Conference on Learning Representations (ICLR)*, 2019.

[3] B. Chu, V. Madhavan, O. Beijbom, J. Hoffman, and T. Darrell. Best practices for fine-tuning visual classifiers to new domains. In *ECCV Workshop TASK-CV: Transferring and Adapting Source Knowledge in Computer Vision*, 2016.

[4] Y. Ganin and V. Lempitsky. Unsupervised domain adaptation by backpropagation. In *International Conference on Machine Learing (ICML)*, 2015.

[5] Y. Ganin, E. Ustinova, H. Ajakan, P. Germain, H. Larochelle, F. Laviolette, M. Marchand, and V. Lempitsky. Domain-adversarial training of neural networks. *Journal of Machine Learning Research (JMLR)*, 2016.

[6] P. Isola, J.-Y. Zhu, T. Zhou, and A. A. Efros. Image-to-image translation with conditional adversarial networks. In *Conference on Computer Vision and Pattern Recognition (CVPR)*, 2017.

[7] M. Jaderberg, K. Simonyan, A. Zisserman, and K. Kavukcuoglu. Spatial transformer networks. In *Conference on Neural Information Processing Systems (NIPS)*, 2015.

[8] A. Krizhevsky. Learning multiple layers of features from tiny images. Technical report, University of Toronto, 2009.

[9] Y. LeCun and C. Cortes. MNIST handwritten digit database. http://yann.lecun.com/exdb/mnist/.

[10] D. Li, Y. Yang, Y.-Z. Song, and T. M. Hospedales. Deeper, broader and artier domain generalization. In *International Conference on Computer Vision (ICCV)*, 2017.

[11] D. Martin, C. Fowlkes, D. Tal, and J. Malik. A database of human segmented natural images and its application to evaluating segmentation algorithms and measuring ecological statistics. In *International Conference on Computer Vision (ICCV)*, 2001.

[12] Y. Netzer, T. Wang, A. Coates, A. Bissacco, B. Wu, and A. Y. Ng. Reading digits in natural images with unsupervised feature learning. In *NIPS Workshop on Deep Learning and Unsupervised Feature Learning*, 2011.

[13] O. Russakovsky, J. Deng, H. Su, J. Krause, S. Satheesh, S. Ma, Z. Huang, A. Karpathy, A. Khosla, M. Bernstein, A. C. Berg, and L. Fei-Fei. ImageNet Large Scale Visual Recognition Challenge. *International Journal of Computer Vision (IJCV)*, 2015.

[14] TensorNets. https://github.com/taehoonlee/tensornets.